Magnetic Resonance Technologies Based on Reverse Polarization for Image-Guided Interventions

A THESIS
SUBMITTED TO THE DEPARTMENT OF ELECTRICAL AND ELECTRONICS ENGINEERING
AND THE INSTITUTE OF ENGINEERING AND SCIENCE
OF BILKENT UNIVERSITY
IN PARTIAL FULFILLMENT OF THE REQUIREMENTS
FOR THE DEGREE OF
DOCTOR OF PHILOSOPHY

By
Haydar Çelik
October, 2010

I certify that I have read this thesis and that in my opinion it is fully adequate, in scope and in quality, as a thesis for the degree of doctor of philosophy.

_____

Prof. Dr. Ergin Atalar (Supervisor)

I certify that I have read this thesis and that in my opinion it is fully adequate, in scope and in quality, as a thesis for the degree of doctor of philosophy.

_____

Prof. Dr. Ayhan Altıntaş

I certify that I have read this thesis and that in my opinion it is fully adequate, in scope and in quality, as a thesis for the degree of doctor of philosophy.

_____

Prof. Dr. Nevzat G. Gençer

I certify that I have read this thesis and that in my opinion it is fully adequate, in scope and in quality, as a thesis for the degree of doctor of philosophy.

Assoc. Prof. Dr. Vakur B. Ertürk

I certify that I have read this thesis and that in my opinion it is fully adequate, in scope and in quality, as a thesis for the degree of doctor of philosophy.

Assist. Prof. Dr. Ömer İlday

Approved for the Institute of Engineering and Sciences:

Prof. Dr. Levent Onural
Director of Institute of Engineering and Sciences

ACKNOWLEDGMENTS

It is my pleasure to express my sincere gratitude to my supervisor, Prof. Ergin Atalar, whose expertise, understanding, and patience, added considerably to my graduate experience. I appreciate his vast knowledge and skill in all areas of MRI. I am deeply indebted to him.

I would like to thank the members of my thesis committee, Prof. Ayhan Altıntaş, Prof. Nevzat G. Gençer, Assoc.Prof. Vakur B. Ertürk, and Assist. Prof. Ömer İlday for reading and commenting on this thesis.

I am obliged to thank my co-researchers Dr.Namık Şengezer, Doğaç Gülnerman, Davut İbrahim Mahçiçek, Burak Akın.

I am grateful to Emre Kopanoglu for their valuable discussions. I am also grateful to Volkan Acikel, Ozay Hirlakoglu Prof.Dr. Turgut Talı, Dr.Aslı Ulutürk, Vet.Dr. Burcu İnsal Cingöz, M.Can Kerse, Taner Demir, Dr.Okta Algın, Dr.Katja Dörschner, Dr.Aslihan Ors, Gizem Kucukoglu, Yiğitcan Eryaman, Aydan Ercingöz for their supports during studies.

I would also like to thank my family and my love for the support they provided me through my entire life.

ABSTRACT

Magnetic Resonance Technologies Based on Reverse Polarization for Image-Guided Intervention

Haydar Çelik
Ph.D. in Electrical and Electronics Engineering
Supervisor: Prof. Dr. Ergin Atalar
October, 2010

In this PhD dissertation, we presented four magnetic resonance (MR) technologies established upon reverse polarization for image guided interventions. The first three studies are based on tracking interventional devices, such as catheters, biopsy needles, and guidewires. The interventional devices cannot be seen using MRI without markers, coils, or extra devices. Our studies utilize different imaging modalities in order to obtain positional information of the interventional devices. The last study is a novel inductively coupled radio frequency birdcage coil design, which is a miniaturized version of a widely used volume coil. The new design can be used for prostate biopsy or imaging intestines.

The reverse polarization is a mode of magnetic field that is not sensitive to anatomy signal. Therefore, it had been useless until the introduction of the reverse polarization concept. Using a linearly polarized inductively coupled radio frequency (ICRF) coil enables the reverse polarization mode, because a linearly polarized signal consists of both forward and reverse

polarization signals. As a result, building the ICRF coil to interventional devices paves the way of using this method in interventional MRI.

Performances of developed technologies were tested in phantom, animal, and volunteer studies. We believe that the studies explained in this dissertation contribute to obtaining better imaging systems.

Key words: Magnetic resonance imaging, interventional MRI; catheter tracking; fiducial marker, inductively coupled RF (ICRF) coil, transmit array system, birdcage coil

ÖZET

Görüntü Rehberli Girişimler İçin Ters Kutuplaşma Temelli Manyetik Rezonans Teknolojileri

Bu doktora tezinde görüntü rehberli girişimler için ters kutuplaşma tabanlı dört manyetik rezonans (MR) teknolojisi sunulmuştur. İlk üç çalışma kateter, biyopsi iğnesi, ve rehber tel gibi girişimsel cihazların takibine dayanmaktadır. Girişimsel cihazlar üzerlerine işaret, sargı, ya da fazladan cihaz yerleştirilmeden MR görüntüleme (MRG) ile görüntülenememektedir. Çalışmalarımız, girişimsel cihazların konum bilgilerini elde edebilmek için farklı görüntüleme yöntemlerinden faydalanmaktadır. Son çalışmamız sıklıkla hacim sargısı olarak kullanılan kuşkafesi tasarımının yeni bir şekli olarak indükleyerek eşlenmiş radyo frekans (İERF) sargısı olarak kullanımına dayanır. Bu yeni tasarım prostat biyopsisi ya da bağırsakların görüntülenmesinde kullanılabilir.

Ters kutuplaşma, manyetik alanın insan anatomisi sinyaline duyarlı olmadığı bir modudur. Bu nedenle, ters kutuplaşma kavramının ortaya atılmasına kadar işe yaramaz olduğu kabul edilmiştir. Düz kutuplaşmış olan indüklenmeyle eşleşmiş radyo frekansı (İERF) sargılarının kullanılması, ters kutuplaşma modunu işe yarar hale getirmiştir, çünkü düz kutuplaşmış bir manyetik alan hem düz hem de ters kutuplaşmış manyetik alanları içinde barındırır.Sonuç olarak, İERF sargılarının girişimsel aletlere monte edilmesiyle bu metodun girişimsel MR görüntülemede kullanılmasının yolu açılmıştır.

Sunulan çalışmaların başarısı fantom, hayvan, ve gönüllü çalışmalarında denenmiştir. Bu tezdeki çalışmaların daha iyi görüntüleme sistemleri elde etmeye katkı sağlayacağına inanıyoruz.

Anahtar sözcükler: Manyetik rezonans görüntüleme, girişimsel MRG, kateter izleme; işaretleyici, indükleyerek eşlenmiş radyo frekans sargısı, sıralı gönderim sistemi, kuşkafesi sargısı.

Contents

List of Figures

imager bore between them. Two probes were placed on the tips of the coils and another one was placed midway between the coils as a reference data probe. In the heating experiment we used fast SPGR with TR of 6.5 ms and flip angle of 90 ^{o} for duration of 690 seconds.

Figure 2.7: Plot of the heating experiment. A temperature rise of 2.4°C was seen in 690 seconds in the reference location. A sharp increase in temperature (15°C in 100 seconds) at the tip of the ICRF coil was observed. This implies local heating around the tuning capacitor; the temperature increased by 20°C over 320 seconds. However the RCRF coil heated much less (4.1°C in 690 seconds).

Figure 2.8: Phantom imaging experiment. The forward polarization mode of images, the reverse polarization mode of images, and the color-coded images are in the left, the middle, and the right columns respectively. The first row shows images with a flip angle of 1^{o}. Although a low flip angle was used, the catheter appeared bright suggesting flip angle amplification. In this low flip-angle imaging case, the RCRF coil worked as an ICRF coil and a high contrast between the RCRF coil signal and the background signal was achieved.

As the flip angle was increased (second and third rows in Figure 2.8), the background signal intensity increased. No overtipping artifact (flip angles more than 90^{o}) around the catheter was observed. This suggested a successful decoupling by the back-to-back diodes. However, image contrast is significantly decreased.

Under all conditions, our algorithm worked successfully, as shown by the reverse polarization images (middle column in Figure 2.8). The background signal is almost completely suppressed in all cases. Color-coded images allowed visualization of the catheter and the background.

Figure 2.9: The animal imaging experiment with fast gradient echo sequence. As in the phantom imaging experiment images, the forward polarization mode, the reverse polarization mode and the color-coded images are shown from left to right. Figures were acquired using slice thicknesses of 5 mm, 20 mm, and without slice selection.

In the first row (gradient echo images with slice thickness of 5 mm and flip angle of 1o), the catheter can be easily seen in the forward polarization mode image; background signal suppression was almost perfect in the reverse polarization mode image. On the other hand, with flip angle of 40^{o}, the catheter was barely visible in the forward polarization mode image, and background signal suppression was almost complete in the reverse polarization mode image. Color coding enabled visualization of both catheter and background.

As the slice thickness was increased (20 mm in Panel b, no slice selection in Panel c), visibility of the catheter decreased significantly in the forward polarization mode image even with a flip angle of 1o. Identification of the catheter was almost impossible in the forward polarization mode image when a flip angle of 40^o was used. On the other hand, background suppression was effective in both reverse polarization mode images. Again, the color-coding method enabled visualization of the catheter against the background.

Figure 2.10: The animal imaging experiment with SSFP sequence. SSFP sequence is frequently used in guidance of interventional procedures. As expected, visibility of the catheter in SSFP sequence was low in the forward polarization mode image; on the other hand, background suppression in the reverse polarization mode image was successful.

Figure 3.1: Sketch of the n^{th} element of the phased array coil, CRF coil, and spin interactions. a) $\vec{B}_n$ is the magnetic field generated by the n^{th} element of the receive phased array coil at the point of interest when the unit current, I, is applied to the terminals of the coil element. b) $\vec{M}$ is the rotating magnetization vector of spins and $\vec{M}_{CRF}$ is the magnetization vector of the CRF coil that is oscillating in a linear trajectory. The spins around the CRF coil induce a current, I_{CRF}. This current on the small CRF coil can be represented by a magnetization vector, $\vec{M}_{CRF}$. As a result of these magnetizations, a voltage, v_n, is induced on the terminals of the external coil. c) $\vec{B}_c$ is the magnetic field generated by the CRF coil at a point of interest when a unit current, I, is applied to an imaginary terminal of the coil. θ is the orientation angle of the w.r.t x-axis of the CRF coil, and Z is the impedance at this imaginary terminal of the CRF coil.

Figure 3.2: The CRF coil design.

Figure 3.3: Sketch of the NaCl solution phantom and a volunteer for fiducial marker visualization**.**

Figure 3.4: Oblique images of the phantom. (a) The forward polarization mode of the image, (b) the reverse polarization mode of the image, and (c) the color-coded image. Although there is a KCl solution-filled straw as a disturber, the reverse polarization method can separate the RCRF coil from the phantom.

Figure 3.5: Sagittal images of the phantom and ICRF coils. (a) The forward polarization mode of the image, (b) the reverse polarization mode of the image, and (c) the color-coded image. Although the phantom and contrast agent signals are stronger than the ICRF coil signal (left column), the reverse polarization method using the transmit array system suppresses all the signals other than the linearly polarized signal of the ICRF coil.

Figure 3.6: a) Oblique images of the phantom and ICRF coils. (a1) The forward polarization mode of the image, (a2) the reverse polarization mode of the image, and (a3) the color-coded image. Similar to the previous case shown in Figure 3., the method successfully singles out the RCRF coil signal. However, because of the transmission decoupling, the RCRF signal is weaker than the ICRF coil signal.
b) Transversal images of the ICRF coil, RCRF coil, and KCl solution. (b1) The forward polarization mode of the image, (b2) the reverse polarization mode of the image, and (b3) the color-coded image. Although the phantom and contrast agent signals are stronger than the ICRF coil signal (left column), the reverse polarization method using the transmit array system suppresses all signals other than the linearly polarized signal of the ICRF coil.

Figure 3.7: a) Oblique image of the receive array. (a1) The forward polarization mode of the image, (a2) the reverse polarization mode of image, and (a3) the color-coded image.
b) Oblique image of the transmit array.(b1) The forward polarization mode of the image, (b2) the reverse polarization mode of the image, and (b3) the color-coded image. Similar to the receive array case, suppression of the anatomy signal for MR guidance is effective.

Figure 3.8: a) Transversal image of receive array coil. (a1) The forward polarization mode of the image (a2), the reverse polarization mode of the image, and (a3) the color-coded image.
b) Transversal image of transmit array. (b1) The forward polarization mode of the image, (b2) the reverse polarization mode of the image, and (c3) the color-coded image.

Figure 3.9: a) Sagittal image of receive array coil. (a1) The forward polarization mode of the image (a2), the reverse polarization mode of the image, and (a3) the color-coded image.
b) Sagittal image of transmit array. (b1) The forward polarization mode of the image, (b2) the reverse polarization mode of the image, and (c3) the color-coded image.

Figure 4.1: A conventional MRI RF excitation and the field polarization using a single channel body birdcage coil with a quadrature hybrid. The quadrature hybrid divides input excitation signal into two halves with 90^o phase difference. This excitation enables a forward polarized field inside a birdcage coil.

Figure 4.2: Standard spoiled GRE sequence RF pulse schemes and the birdcage coil excitation using the transmit array system. If the quadrature hybrid is eliminated and two excitation channels are input with a same spoiled GRE excitation pulses a linearly polarized field is created inside the birdcage coil.

Figure 4.3: The modified RF excitation scheme and the birdcage coil field using the transmit array system. Excitations of the channels change such that a linearly polarized field with a turning polarization vector is created.

Figure 4.4: a) Interaction of the linear polarized RF and the ICRF coil. b) k-space lines result of circulating polarization vector.

Figure 4.5: Simulation results of TrueFISP sequence.

Figure 4.6: a) Phantom setup. The same phantom was used for imaging experiments. b) Result of the rotational orientation experiment.

Figure 4.7: Transversal images of the method with varying number of turns, *N*. Images show that the amount of shifting pixel can be adjusted. a) Original image $P = 1$. b) $P = 16$. c) $P = 8$.

Figure 4.8: Color-coded images with changing parameters. a) Polarization vector turns counter-clockwise direction and phase encoding direction is A-P. b) Polarization vector turns clockwise direction, same phase encoding direction with a. c) Polarization vector turns counter-clockwise direction and phase encoding direction is L-R.

Figure 4.9: Color-coded images of different planes. a) Coronal image. b) Sagittal image. c) Oblique image.

Figure 4.10: Imaging experiment results of TrueFISP sequence. a, b, and c shows transversal images with different oil and KCl solutions. a) High oil signal intensity. b) High KCl solution intensity with suppressed oil signal. c) Highest KCl solution signal intensity with residual oil signal. d) Oblique plane with low oil signal intensity. e) Coronal plane with low background signal intensity.

Figure 5.1: Simulation of eight legs highpass inductively coupled birdcage coils. a) Forward mode of ICBC b) Reverse mode of ICBC.

Figure 5.2: A picture of the high-pass inductively coupled birdcage coil used in experiments.

Figure 5.3: A picture of the high-pass ICBC coil. Capacitors can be placed inside, outside, and on the endrings. Here, the capacitors are placed inside of the coil.

Figure 5.4: Tuning method of the coupled birdcage coils.

Figure 5.5: Window/Level are the same for all images. a) Axial image of mode 1 b) Sagittal image of mode 1 c) Axial image of mode 2 d) Sagittal image of mode 2.

Figure 5.6: Window/Level are the same for all images. a) Axial image of mode 1 b) Sagittal image of mode 1 c) Axial image of mode 2 d) Sagittal image of mode 2.

1. INTRODUCTION

Surgical procedures are performed for the direct visualization of possible diseases and for the treatment during the procedure. However, these procedures carry risks due to the direct exposure of the internal parts of human body. As an example, a by-pass operation needs an open surgery which may cause contamination. Interventional radiology is a profession that consists of minimally invasive procedures using radiological images. The purpose of the interventional radiology can be diagnostic and/or treatment with minimally invasive methods. Images are used to guide interventional devices such as biopsy needles, catheters, and guide-wires. Therefore, using minimally invasive interventional radiology methods minimizes infections and recovery times.

Precise and fast localization of the interventional devices is a necessity to perform minimally invasive operations. In order to acquire images for guidance, different modalities are used in interventional radiology. Ultrasound is inexpensive but suffers from poor contrast. Today, catheter based X-ray procedures are commonly used with high success rates for the treatment of wide range of illnesses. Although X-ray provides almost perfect visualization of the interventional devices, the soft tissue contrast is very poor and only very skilled operators can perform these procedures successfully [1]. Furthermore, not only patients, but also staffs are exposed to high dose of ionizing radiation which may cause long term health problems. As compared to other imaging techniques, MRI is a non-ionizing modality and a very promising option for the accurate guidance of the complicated interventional procedures providing high soft tissue contrast. However, visualizing the interventional devices using MRI is rather difficult as opposed to X-ray. Therefore many tracking techniques have been developed. Paramagnetic materials [1-3], contrast agents [4-6], and other local signal manipulators [7, 8] are the main passive tracking tools. Automatic identification of the position of the catheter in passive tracking techniques [9] is difficult, because, these approaches typically yield weak contrast. Alternatively, it is also possible to obtain an image of both the catheter and the background simultaneously with active techniques [10, 11] which also address the contrast issue [12-20]. However, in that case, the catheter needs to be electrically connected to the MR scanner and this may cause radio frequency (RF) safety problems as well as difficulties in handling the device. There are also hybrid methods which make use of an inductively coupled RF (ICRF) coil [21]. ICRF coils [22] are simple wire loops made resonant using a capacitor. A

transmit field induces current on the ICRF coil that amplifies the excitation field in its vicinity and creates MRI signal amplification. These coils have been used for small field of view (FOV) imaging [23, 24] as well as catheter tracking [21, 25]. In our studies, we aimed to improve the interventional device visibility using the ICRF coils and reverse polarization method.

The reverse polarization method is related to precession direction of spins under a DC magnetic field. Spins are fundamental characteristic property of particles and when they are exposed to a torque under a DC magnetic field they precess and this precession causes magnetization and angular momentum. Direction of the precession is dependent on the direction of the DC magnetic field with the left hand rule. In MRI, DC magnetic field is B_o and its direction is on the *z*-axis. We call the precession of spins in MR scanner as forward polarization. Spins can be excited by a forward polarized field and a coil, which is sensitive to forward polarized field, can receive signal due to spin precession. Coils are MR hardware components that transmit magnetic field to excite spins and/or receive magnetic field created by spins in human body. On the other hand, a reverse polarized excitation cannot excite spins and also a coil with reverse polarized sensitivity cannot receive signal of the spins.

The first three studies in this dissertation are mainly related to catheter tracking. The reverse polarization method is introduced in the second chapter. Its implementation to transmit and phased array coils are explained in the third chapter. Circulating linear polarization vector using transmit array system will be discussed in the forth chapter. A novel inductively coupled birdcage coil design is the subject of the fifth chapter.

In the second chapter of the thesis, an ICRF coil visualization method, which allows separation of the catheter and the anatomical information by using the reverse and forward polarization modes of a receive-only birdcage coil, is proposed. Birdcage coils are very common cylindrical shaped volume coils that is used to image subject inside the coil. The reverse polarization method allows images of the anatomy and the catheter to be combined into a color-coded image where color-coding is used to monitor the catheter signal during interventions. Quadrature hybrids are passive devices that are used in birdcage coils in order to obtain forward polarized magnetic field excitation and reception. In our method, a receive-only birdcage coil without a quadrature hybrid was constructed and then it was connected to a

scanner as a two-channel phased array receive coil in order to reconstruct both forward and reverse polarized images simultaneously. MR signals acquired from the two channels were added after phase adjustments to create the reverse and forward polarization modes images. The reverse polarization mode image contained signal only from the ICRF coil, but the forward polarization mode displayed both the anatomical information and the ICRF coil.

In all of the MRI applications and methods explained above, a conventional imaging system has been used. In these systems, there is a single channel RF transmit birdcage body coil that produces forward polarized rotational field. This field is used to flip spins in the anatomy. The signal originates from the anatomy due to the transmit coil excitation and it is received by different RF coil types. A body coil is a single channel transmit coil, but at the same time it can be used as a single channel receive coil. On the other hand phased array coils are multi-channel RF receive coils and weights can be optimized to increase signal-to-noise ratio (SNR). Transmit array systems have recently been introduced for experimental studies. These systems enable multi-channel RF transmission. Similar to the multi-channel reception case, such a system can be optimized for higher SNR. However, transmit array studies are mostly concentrated on understanding the working principles, exploring the capabilities of the system, and homogenizing B_1 fields at high frequencies. Therefore, usage of the transmit array system has been limited. In our second study, we attempt to improve the visibility of the interventional devices by implementing the reverse polarization method to not only phased array but also transmit array coils. Two different applications of the reverse polarization method are presented in this part: a) catheter tracking and (b) fiducial marker visualization, in both of which transmit and receive arrays are used.

Our third study in the forth chapter proposes a novel method for i) the detection of rotational orientation, and ii) the position tracking of an ICRF coil using a transmit array system. The method can be used with an interventional device (such as catheters and guidewires) on which an ICRC coil is constructed. In this study, a conventional body birdcage coil is used, but the quadrature hybrid is eliminated for a two channel transmission similar to the first and the second studies. This study may look very similar to the reverse polarization method mentioned above, but in this method, conventional sequences were modified and excitation scheme was changed during the acquisition. Furthermore, the transmit array system provided two identical RF pulses with different phase and amplitude at each repetition time (TR) in order to obtain

linearly polarized excitations instead of conventional forward polarized rotational excitation. Responses of the anatomy and the ICRF coil to this RF excitation scheme are different such that they can be separated in real-time. After separating the devices from the anatomy signal, a color-coded image is reconstructed. More importantly, this novel method enables to calculate the absolute orientation of the ICRF coil constructed on a catheter in real-time without any extra cost. Even though many researchers tried to deal with the tracking problem, only Anderson et al. tried to address a solution for the rotational orientation issue using phase images of active micro coils manually [26]. The rotational orientation information may increase the control on the catheter and can be extremely useful for several applications, such as MR-guided intravascular focused ultrasound (IVUS) [27, 28] with independent transducer arrays [29] and RF ablation. FLASH (Fast Low Angle SHot Magnetic Resonance Imaging) [66] and TrueFISP (True fast imaging with steady state precession) [67] are two different fast sequences commonly used in real-time applications. An MR sequence is a set of RF and gradient magnetic pulses and time spacing between these pulses. Sequences are used in conjunction with gradient fields and MR signal reception to produce MR images. Modified FLASH and TrueFISP sequences are used for tracking experiments. Nevertheless, only the FLASH sequence is used to detect rotational orientation of the catheter. The acquired images using the method we present show the feasibility of the different applications, such as the catheter-tracking. Furthermore, rotational orientation information of the catheter is important in some of the applications, such as MR guided endoluminal focused ultrasound, RF ablation, side looking optical imaging, and asymmetric needle puncturing. The method we introduced in this chapter makes these applications feasible.

In the applications explained above, the birdcage coil has been mentioned and used as a volume coil, i.e. subjects are placed inside the coil, because, the field of an inner volume of a birdcage coil is very homogeneous. However, using outside of the birdcage coil has not been considered by researchers because of its size and shape (Figure 2.1). In the fifth chapter, a new miniaturized birdcage coil design without any matching and active decoupling circuits, amplifiers, and wire connectors, is introduced. Similar to the inductively coupled RF coils, the standalone birdcage coil design couples to the external coils inductively. The main advantage of the standalone design is being independent from scanner manufactures. The new design can be used as an internal imaging coil and catheter tracking.

MRI is a very promising modality for minimally invasive interventional procedures. In this dissertation, solutions and improvements for interventional MRI using reverse polarization are presented. The reverse polarization concept was introduced in order to make use of “useless” component of MRI signal in 2006 [30]. We believe this study will pave a way for better imaging systems for more accurate diagnostics and treatments using the reverse polarization idea.

2. A CATHETER TRACKING METHOD USING REVERSE POLARIZATION FOR MR-GUIDED INTERVENTIONS

.

2.1. Introduction

Magnetic Resonance Imaging (MRI) is a very promising option for accurate guidance of complicated interventional procedures as it provides high soft tissue contrast; however visualizing interventional devices is rather difficult and many tracking techniques have been developed. Automatic identification of the position of the catheter in passive tracking techniques [9] is difficult. But with active techniques [10, 11], it is possible to obtain an image of both catheter and background simultaneously. However, the catheter needs to be electrically connected to the scanner and this may cause RF safety problems and difficulties in handling the device.

In 2005, Quick *et. al*. proposed wireless active catheter visualization [21] by using an ICRF coil [31]; this can be classified as a hybrid method blending active and passive catheter visualization techniques. A sequence with a small flip angle ($<5^o$) is used to visualize the catheter. The amplified flip angle generates a bright signal around the catheter against a low intensity background image. However, when a sequence with a strong background signal is used, it may be difficult to locate the catheter, and the high flip angles around the catheter become a safety concern. While the safety problems may be eliminated using decoupling techniques during RF transmission, the flip angle amplification property of the transmit mode will be lost, leaving only the signal amplification in the receive mode which renders visualization of the ICRF coil difficult [32]. In active tracking techniques, this problem has been solved by separate acquisition of the catheter and background signals and by color-coding the images [33, 34].

In this study, a novel technique for catheter tracking using an ICRF coil that allows the separate acquisition of background and catheter images simultaneously is proposed. This

method allows real-time, color-coded display of the ICRF coil on a background image. An in-vivo animal experiment demonstrates the feasibility of the proposed method.

2.2. Theory

In MRI, excited spins generate a rotating magnetic field which can be picked up by a quadrature coil tuned to receive a forward polarized magnetic field. When such a coil is physically reversed or tuned to the reverse polarized magnetic field, no signal can be detected. On the other hand, if the magnetic field is generated by a current on a simple loop instead of excited spins, the field does not rotate; instead it oscillates generating a linearly polarized field. This field can be picked up by quadrature coils tuned either to forward or reverse polarized magnetic fields, because a linearly polarized field can be decomposed into forward and reverse polarized magnetic fields. When a resonating loop is placed on a catheter, excited spins induce current on this loop and its associated magnetic field can be picked up by a quadrature coil tuned to the reverse polarization field.

Note that the same coil cannot detect any signal directly coming from the excited spins. This section outlines the theory behind this phenomenon.

2.2.1. Birdcage Volume Coil

Birdcage [35] coils have been widely used since they were first introduced in 1985 by Hayes *et. al.* They have two main advantages: first, they create homogenous magnetic fields; second, they can easily be built as a quadrature coil.

With a quadrature hybrid circuit, standard quadrature birdcage coils are sensitive to the forward polarized magnetic fields (Figure 2.1a).

This can be explained by the principle of reciprocity: when a unit current is applied to one of the two feeds of the birdcage coil, a uniform magnetic field in $\boldsymbol{x}$-direction is generated, suggesting that the signal received from this feed is the $\boldsymbol{x}$-component of the magnetic field. Similarly, when the other feed is used to receive the MRI signal, it becomes sensitive to the $\boldsymbol{y}$-component of the magnetic field.

If the signal received from feed-2 (***y***-channel) is $\pi/2$ phase-delayed before adding to the other, the coil becomes sensitive to the forward component of the magnetic field. This phase delay can be represented by multiplying by the complex number $-i$.

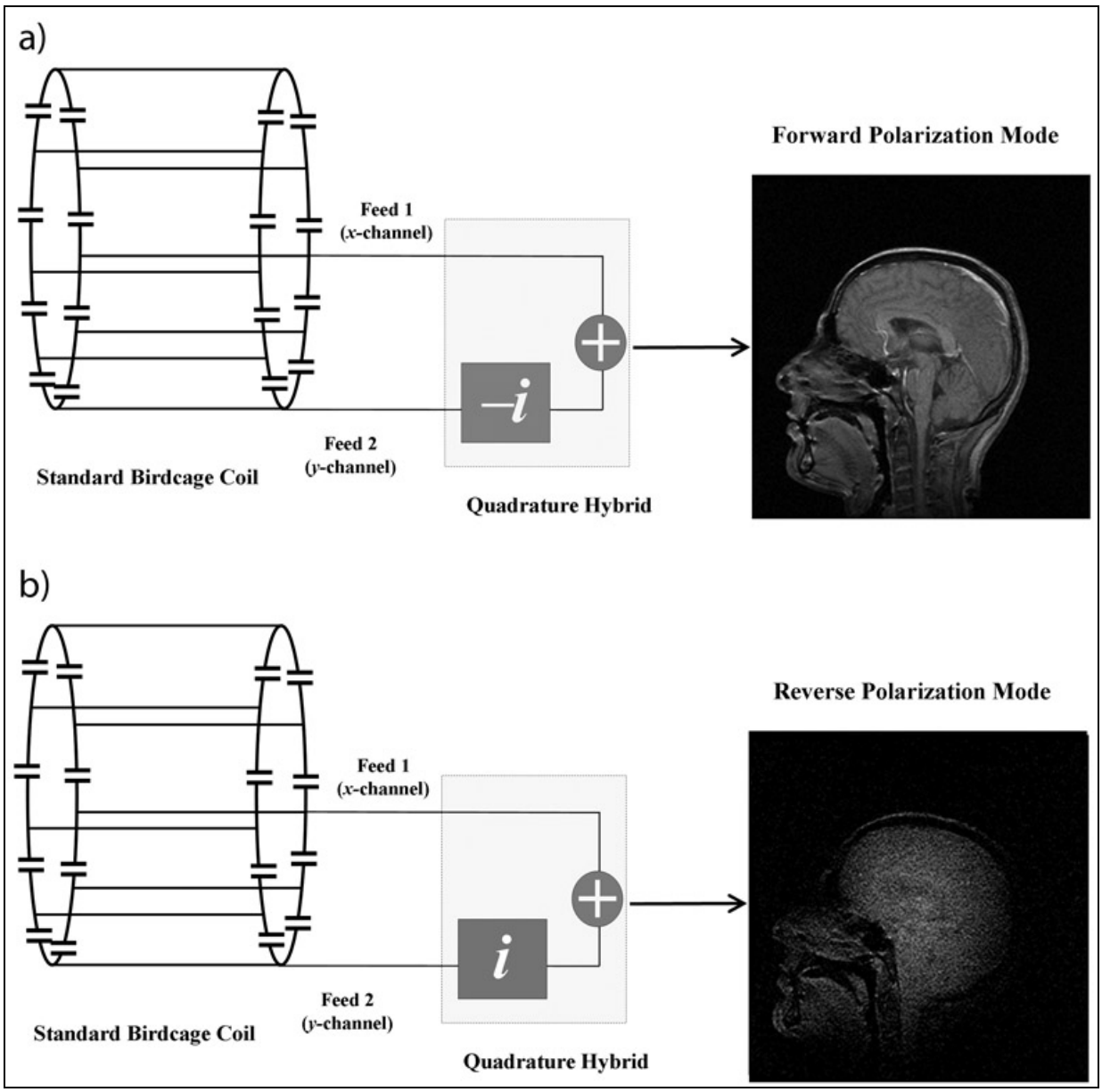

Figure 2.1: a) Standard birdcage coil configuration. The birdcage coil has two feeds and they are connected to a quadrature hybrid. The quadrature hybrid creates a 90^o phase difference between the x and y components of the received signals which are added to obtain the forward polarization mode signal. b) Reverse polarization mode image of a standard birdcage coil. In a perfect system, no MRI signal can be detected, if the phase of the MRI signal from feed 2 (y-channel) is advanced by 90^o before adding. The same effect can be obtained by cross connecting the feeds to the quadrature hybrid connections. However, imperfect systems may result in some signals as seen in the figure. (This figure was taken from [25])

On the other hand, if the feeds of the birdcage coil are connected in reverse order, the signal received from feed-2 (***y***-channel) is $\pi/2$ phase-advanced before adding to the other; this time, the coil becomes sensitive to the reverse component of the magnetic field. This phase delay can be represented by multiplying by the complex number $+i$. Ideally, the resultant image should consist of noise only. However, imperfections in the birdcage coil and quadrature hybrid designs mean that we receive some signals (Figure 2.1b), but the reconstructed image is very noisy.

2.2.2. Soft Quadrature Hybrid

The phase manipulations described above can also be done using software. If image raw data is multiplied by a constant, for example $\boldsymbol{i}$ or $\boldsymbol{e}^{i\pi/2}$, the magnitude of the pixel value will remain unchanged but its phase will advance by $\pi/2$. The addition operation is also very straightforward for a computer program.

If the signals from feeds 1 and 2 are directly acquired, the function of the quadrature hybrid can be imitated by a simple computer program. Thus with a soft-quadrature-hybrid, two images representing forward and reverse polarization modes can be obtained simultaneously. These operations can be completed very rapidly making real-time implementation possible.

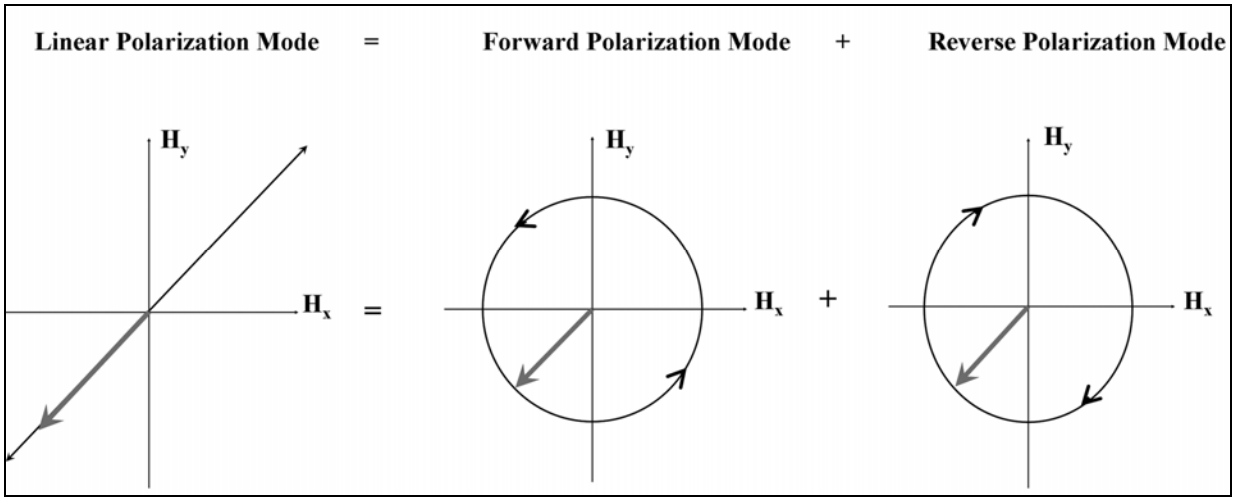

Figure 2.2: The ICRF coil and linear polarization. The MR signal induces current on an ICRF coil and this creates a linearly polarized signal. A linearly polarized signal can be decomposed into forward and reverse polarized signals. Therefore, an ICRF coil functions as a polarization converter. (This figure was taken from [25])

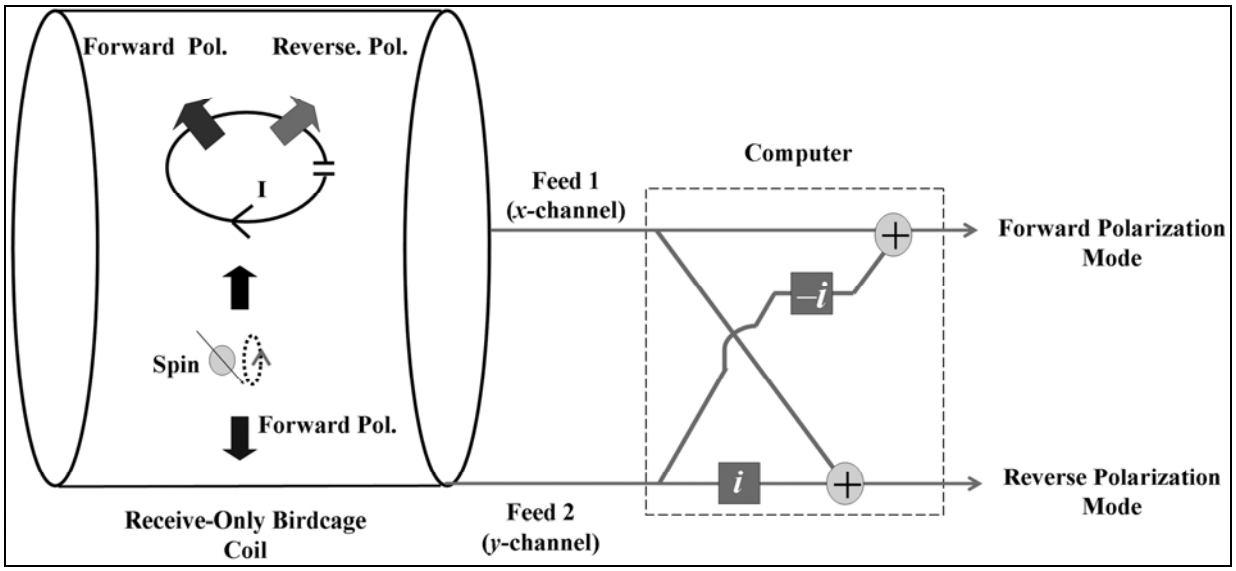

Figure 2.3: Visualizing the ICRF coil and the anatomy. Spins in the anatomy create a forward polarized signal. If an ICRF coil is placed in the RO birdcage coil, spin rotation induces current on the ICRF coil and it creates a linear polarized signal, which consists of both forward and reverse polarized signals. By feeding x and y-channels directly to the scanner, both forward and reverse polarization modes can be reconstructed. (This figure was taken from [25])

2.2.3. Linear Polarization

Spins produce a forward polarized field in the receive-only birdcage coil; therefore in reverse polarization mode, no signal can be detected.

On the other hand, if the magnetic field is generated by a current on a simple loop instead of excited spins, the field oscillates rather than rotating. This linearly-polarized magnetic field can be decomposed into forward and reverse polarized fields and therefore can be detected in both forward and reverse polarization modes (Figure 2.2).

When an ICRF coil is placed inside the birdcage coil, spin rotation induces current on the ICRF coil. This current produces a linearly polarized field allowing us to obtain the ICRF coil image in reverse polarization mode without any signal coming directly from the anatomy (Figure 2.3).

2.4. Method

2.4.1. Receive-Only Birdcage Coil

A conventional high-pass receive-only birdcage coil with 12 legs was built. Diodes were used for decoupling (Figure 2.4)

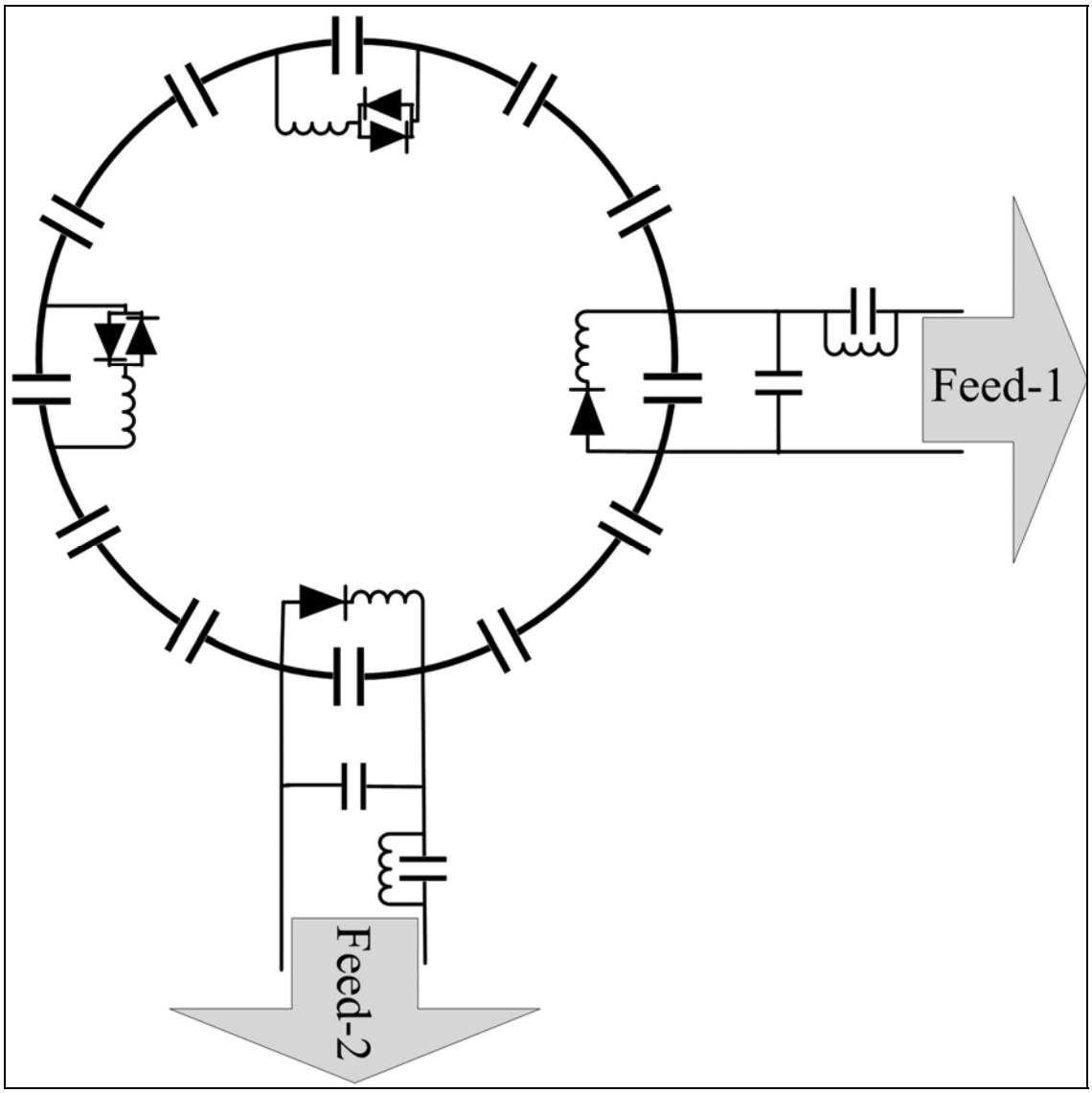

Figure 2.4: Sketch of the upper end-ring part of the receive-only birdcage coil. The receive-only birdcage coil has two feeds and an inductor-diode system is used for decoupling. Scanner-supplied DC current turns on the diode during RF transmission. Two back-to-back diodes are used for passive decoupling. Again, during the RF transmission, AC current on the end-ring turns on diodes which detune the coil, resulting in effective decoupling. (This figure was taken from [25])

In our design, two feeds of the coil were not connected to the quadrature hybrid. A soft-quadrature hybrid system was used instead and the two feeds were directly connected to the dual phased array connector of a 1.5 tesla MR scanner [36 Wisconsin, USA #242]. The acquired data was reconstructed in forward and reverse polarization modes (as described in the Theory section) using a MATLAB code.

2.4.2. Inductively Coupled RF Coil

Two types of ICRF coils were built. The first one did not contain any diodes and therefore it coupled with both RF transmit and receive coils. The coil was 8.5-cm long and constructed on a 2 mm Teflon catheter using coated copper wire 0.4 mm in diameter; a heat shrink tube was used for isolation resulting in a prototype device with an outer diameter of 4 mm (Figure 2.5). It was tuned by a 75 pF ceramic chip capacitor [37] to 63.85 MHz using an HP 8753D network analyzer [38 CA, USA #244]. This design was used only in heating experiments.

The second type of ICRF coil was the same except for a pair of back-to-back BAS70INCT-ND schottky diodes [39] in parallel to the 75 pF tuning capacitor. We call this a receptively coupled RF (RCRF) coil because it couples with the RF receive coils rather than with the transmit coil. The RCRF coil was used in heating experiments as well as in all imaging experiments.

There were two performance criteria in our ICRF coil study: visibility and safety of the coils during any interventional procedure. Quick *et.al* reported that the contrast-to-noise ratio performance obtained using the ICRF coil is higher than the performance obtained using the RCRF coil [32]. However, the RF safety profiles of these coils have not been investigated. Therefore, we tested the RF safety performance of the two coils.

2.4.3. Phantom Heat Experiments

In the safety test, we measured the safety index, i.e. maximum temperature rise for a given specific absorption rate (SAR) as described in [40]. Since the relation between temperature and SAR is approximately linear, this measure gives a result that is independent of test condition.

In order to reduce measurement errors introduced by the temperature measurement device (±0.2°C) we chose to maximize the applied SAR. In the phantom heat experiments, a gel filled bottle was used (Figure 2.6).

Both ICRF and RCRF coils were placed on the inner wall of a 5lt bottle that had a diameter of 21 cm. The bottle was leaned against the bore of the MR scanner.

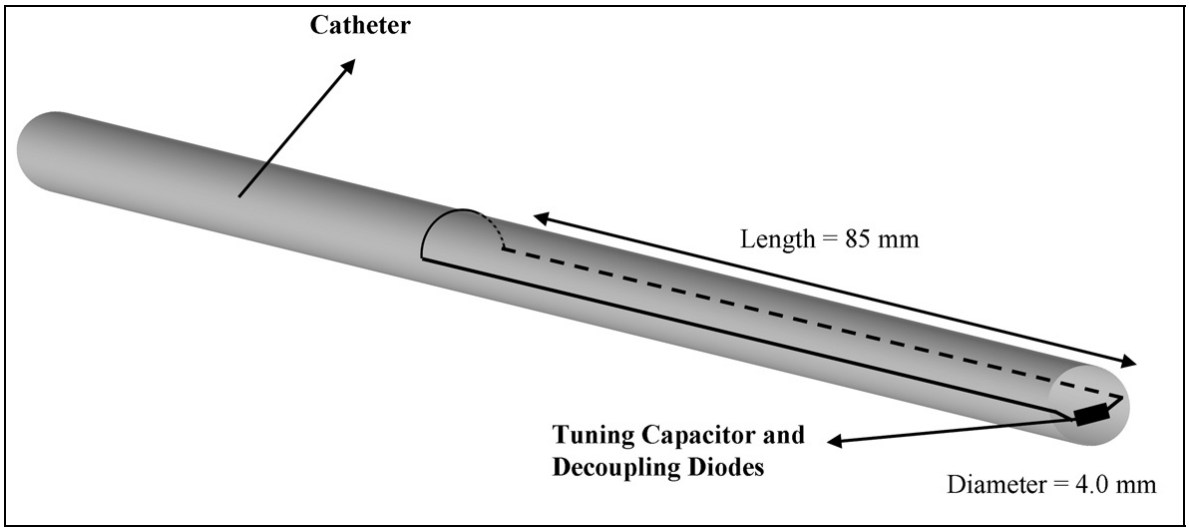

Figure 2.5: The RCRF coil. The RCRF coil has 4.0 mm in diameter and 85 mm long. It is constructed from 0.4 mm diameter coated copper wire. The RCRF coil is tuned by a ceramic chip capacitor to 63.85 MHz using an HP 8753D network analyzer. (This figure was taken from [25])

The heating experiment used fast spoiled gradient echo (SPGR) using the following imaging protocol: echo time (TE): 0.9 ms, repetition time (TR): 6.5 ms, flip angle: 90^{o}, slice thickness: 20 mm, spacing: 0 mm, matrix: 256 X 128, FOV: 480 X 480 mm^2, 15 phases per location, number of excitation (NEX): 60, bandwidth (BW): 62.50 Hz, acquisition duration: 690 seconds.

Neoptix ReFlex 4 channel signal conditioner and T1 fiber optic temperature sensors were used to measure temperature [41 Quebec City, Canada #246]. Since we expected the highest electric field around the capacitor, sensor tips touched the regions where the capacitors were placed. Another sensor was placed on the inner wall of the bottle away from the coils to measure applied maximum SAR (Figure 2.6). At 18.7°C, thermal conductivity, specific heat capacity, and thermal diffusivity of the gel were measured by a KD2Pro thermal properties analyzer [42 USA #247] by simply inserting the needles of the analyzer into the phantom. A sample of the gel is taken from the phantom that had a measured density of 1150 kg/m^3.

As it will be explained in Results section, the RCRF coil was shown to be safer to use and therefore the imaging experiments was conducted using only this type of coil.

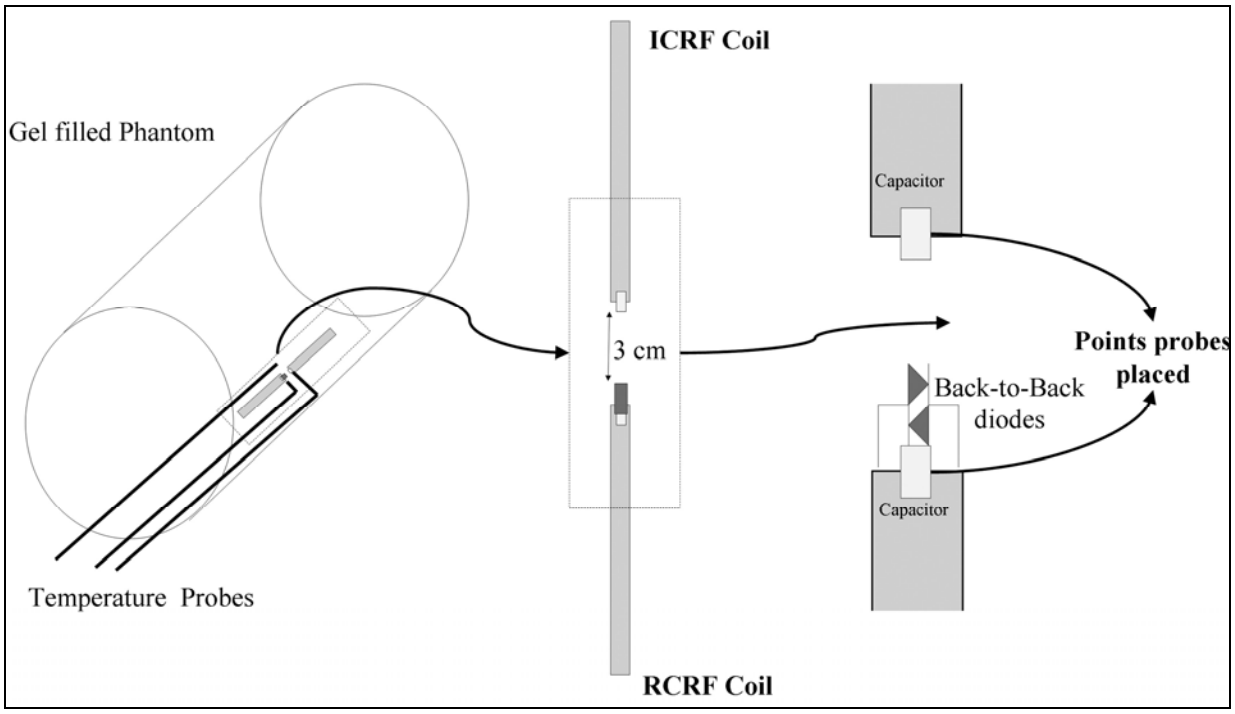

Figure 2.6: Sketch of the heating experiment involving ICRF and RCRF coils. Two coils were placed on the inner wall of the gel filled phantom. The phantom was leaned against the MR imager bore wall in order to obtain maximum heating. The coils were 3 cm from each other with the center of the MR imager bore between them. Two probes were placed on the tips of the coils and another one was placed midway between the coils as a reference data probe. In the heating experiment we used fast SPGR with TR of 6.5 ms and flip angle of 90^o for duration of 690 seconds. (This figure was taken from [25])

2.4.4. Phantom Imaging Experiments

Phantom imaging experiments were conducted to study the reverse polarization technique in ideal conditions. In these experiments, the RCRF coil was inserted into a gel filled bottle. Sagittal images were taken using a gradient echo sequence with several flip angles (1^o, 5^o, and 40^o). The following gradient echo parameters were used: TR/TE: 40/3.4 ms; spacing: 1 mm; slice thickness: 20 mm; matrix: 256 X 256; FOV: 300 X 300 mm^2.

2.4.5. Animal Imaging Experiments

Proof-of-principle animal experiments were done using the RCRF coil. The rabbit esophagus was chosen for ease of implementation [43] and also to test the design in one of the most challenging anatomical structures. Esophagus lies next to trachea, aorta, great veins, lungs and heart. In addition, air inside esophagus makes it difficult to visualize using MRI. The experiments conformed to the Guidelines for the Care and Use of Laboratory Animals, and were approved by the Gazi University ethics committee, Ankara, Turkey. Two New Zealand and two Angora rabbits were used. General anesthesia was induced by intramuscular injection

of 5 mg/kg of ketamine and 40 mg/kg of xylazine. Then the RCRF coil was lubricated and inserted via the mouth into the duodenum. The rabbit was then placed on an MR table and images were taken while the catheter with the RCRF coil was withdrawn through the esophagus. The motion of the tube inside the esophagus was recorded by fast gradient echo and steady state free precession (SSFP) imaging sequences.

The fast gradient echo parameters were: TR/TE: 7/1.9 ms; matrix: 256 X 256; FOV: 300 X 300 $mm^{2;}$ acquisition time: 1.8 seconds. The SSFP parameters were: TR/TE: 6.3/1.7 ms; matrix: 256 X 256; FOV: 300 X 300 mm^2; flip angle: 40^o; slice thickness: 20 mm; acquisition time: 1.6 seconds.

2.5. Results

2.5.1. Phantom Heat Experiments

At 18.7°C, the thermal properties of the gel in the phantom were: thermal conductivity, $K = 0.51$ W/mK ; specific heat capacity, $C = 3820$ KJ/$m^3 K$; thermal diffusivity, $D = 0.13$ mm^3/sec . The density of the gel was 1150 kg/m^3 and hence heat capacity was 4400 J/kg K. Both coils that are described in the Method section were used in phantom heat experiments. A temperature rise of 2.4°C was observed in 690 seconds (Figure 2.7) in the reference location suggesting that the applied SAR was 15 W/kg. Note that the SAR value estimated by the scanner is known to be unreliable [44] when phantoms are used; therefore we used this measured SAR as the applied SAR.

A sharp increase in temperature (15°C in 100 seconds) was observed at the tip of the ICRF coil (Figure 2.7). This implies local heating around the tuning capacitor. The temperature increased by 20°C over 320 seconds. The safety index [40] is calculated to be 1.3°C /(W/kg) In other words, 1.5 W/kg peak power is the maximum that can safely be applied. This will produce a maximum temperature of 2°C while the device is in the body. The temperature of the RCRF coil however increased much less (4.1°C in 690 seconds). The temperature rise was linear in time, and therefore this heating was not local. This suggests that the RCRF coil is much safer to use. Detailed analysis is necessary to determine under what conditions this coil can be scanned safely. As a result of this experiment, we chose to conduct the rest of the experiments using the RCRF coil

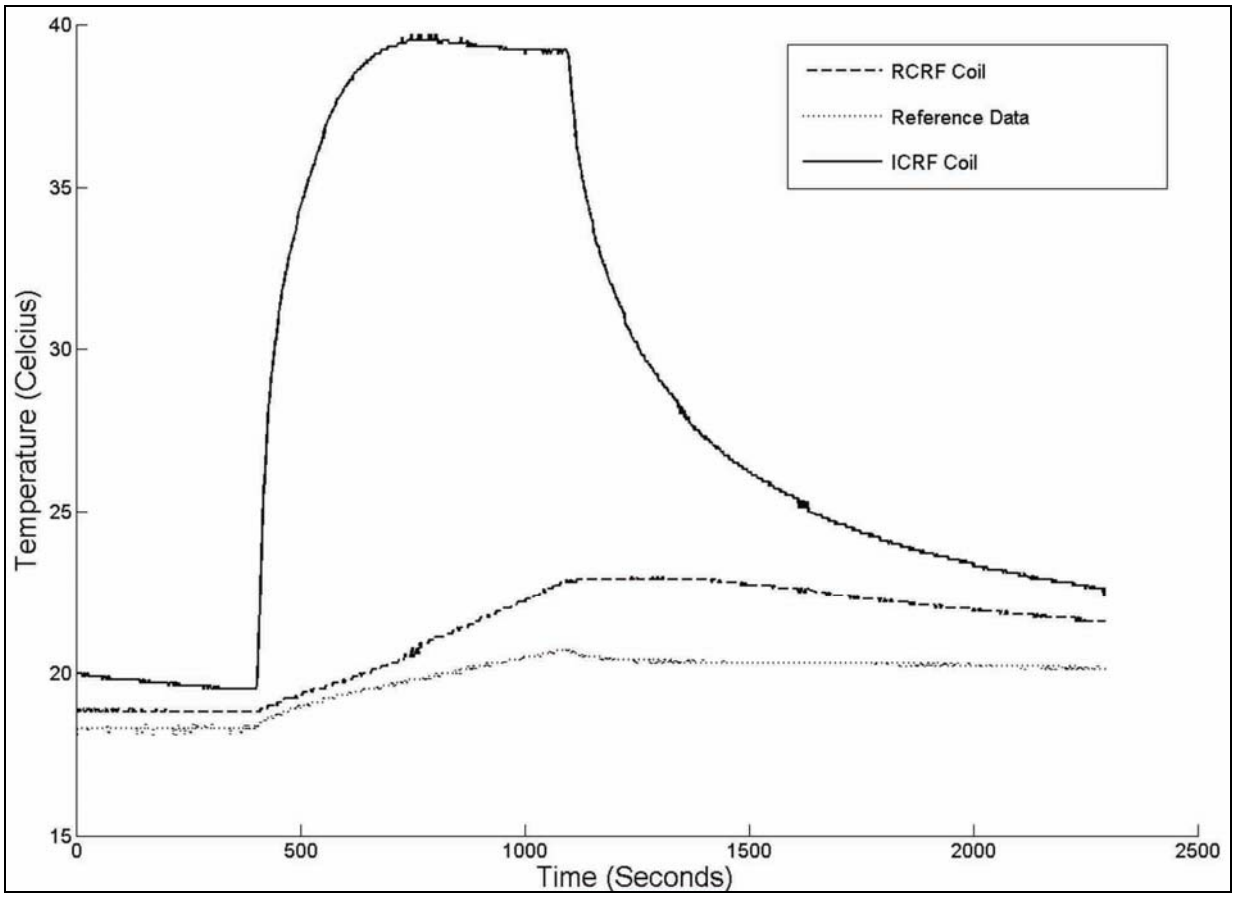

Figure 2.7: Plot of the heating experiment. A temperature rise of 2.4°C was seen in 690 seconds in the reference location. A sharp increase in temperature (15°C in 100 seconds) at the tip of the ICRF coil was observed. This implies local heating around the tuning capacitor; the temperature increased by 20°C over 320 seconds. However the RCRF coil heated much less (4.1°C in 690 seconds). (This figure was taken from [25])

2.5.2. Phantom Imaging Experiments

Figure 2.8 shows the results of the phantom imaging experiments; the forward polarization mode images are in the left column, reverse polarization mode images are in the center, and color-coded images are in the right column. The first row shows images with a 1^{o} flip angle. Although a low flip angle was used, the catheter appeared bright suggesting flip angle amplification. This can be explained by the fact that when a low flip angle is used, induced voltage across the back-to-back decoupling diodes may be lower than their turn-on voltage (0.3 volts for the Schottky diodes). In this low flip-angle imaging case, the RCRF coil worked as an ICRF coil so that high contrast was achieved between the RCRF coil signal and the background signal. As the flip angle was increased (second and third rows in Figure 2.8), background signal intensity increased. No overtipping artifact (flip angles more than 90^{o}) was

observed around the catheter, which means a successful decoupling by the back-to-back diodes was accomplished; however, image contrast was decreased significantly.

In all conditions, our algorithm worked successfully as can be seen in the reverse polarization images (middle column in Figure 2.8). The background signal is almost completely suppressed in all cases. The color-coded images enabled visualization of the catheter and the background.

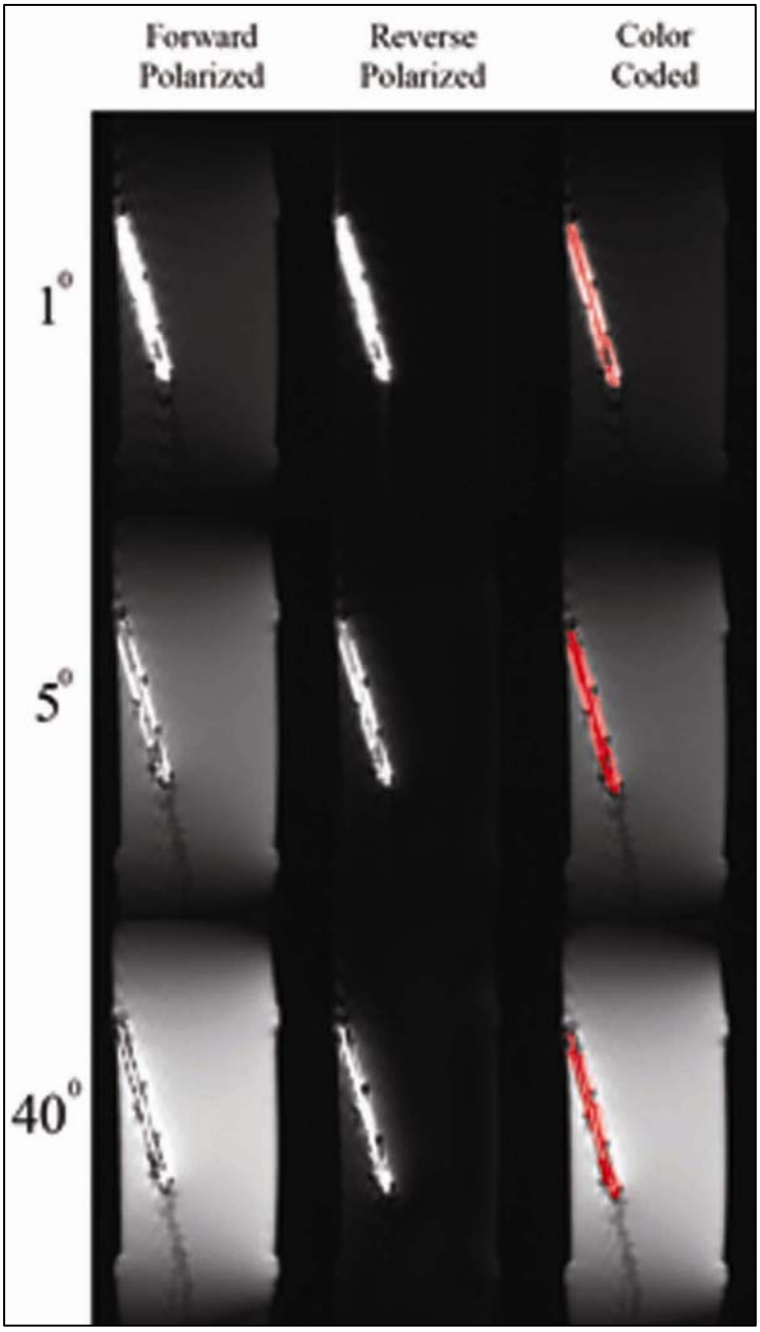

Figure 2.8: Phantom imaging experiment. The forward polarization mode of images, the reverse polarization mode of images, and the color-coded images are in the left, the middle, and the right columns respectively. The first row shows images with a flip angle of 1°. Although a low flip angle was used, the catheter appeared bright suggesting flip angle amplification. In this low flip-angle imaging case, the RCRF coil worked as an ICRF coil and a high contrast between the RCRF coil signal and the background signal was achieved.
As the flip angle was increased (second and third rows in Figure 2.8), the background signal intensity increased. No overtipping artifact (flip angles more than 90°) around the catheter was observed. This suggested a successful decoupling by the back-to-back diodes. However, image contrast is significantly decreased.
Under all conditions, our algorithm worked successfully, as shown by the reverse polarization images (middle column in Figure 2.8). The background signal is almost completely suppressed in all cases. Color-coded images allowed visualization of the catheter and the background. (This figure was taken from [25])

2.5.3. Animal Imaging Experiment

The phantom has a uniform structure; therefore, the RCRF coil can be separated from the phantom easily. However, this is not the case in animal experiments because of the complex structure of tissues. As slice thickness and flip angle increase, visualizing the catheter becomes harder with standard imaging techniques.

Figure 2.9 shows the results of the rabbit experiments. As in the images from the phantom imaging experiment, the forward polarization mode of images, the reverse polarization mode of images and color-coded images are shown from left to right. Figures 2.9a-c are fast gradient echo images, acquired using slice thicknesses of 5 mm, 20 mm, and without slice selection. In addition, SSFP sequence images are shown in Figure 2.9d; these are frequently used to guide interventional procedures. In the first row (gradient echo images with a slice thickness of 5 mm and a flip angle of 1^{o}), the catheter can be easily seen in the forward polarization mode image; in the reverse polarization mode image, background signal suppression was almost perfect. But with a flip angle of 40^{o}, the catheter was barely visible in the forward polarization mode image, and the background signal suppression was almost complete in the reverse polarization mode image. Color-coding enabled visualization of the catheter against the background.

As slice thickness was increased (20 mm in Figure 2.9b, no slice selection in Figure 2.9c), visibility of the catheter decreased significantly in the forward polarization mode image even with a flip angle of 1^{o}. Identification of the catheter was almost impossible in the forward polarization mode image when a flip angle of 40^{o} was used. On the other hand, background suppression was effective in both reverse polarization mode images. Again, color-coding enabled visualization of the catheter within the background. As expected, visibility of the catheter in the SSFP sequence was low in the forward polarization mode image, but background suppression in the reverse polarization mode image was successful (Figure 2.9d).

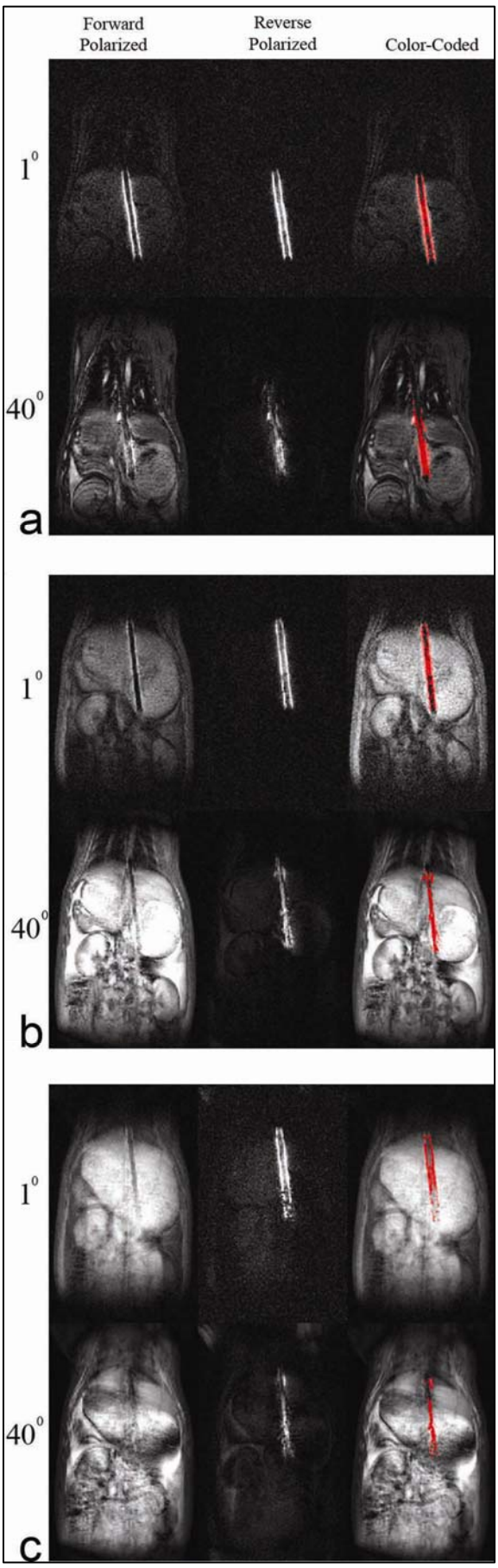

Figure 2.9: The animal imaging experiment with fast gradient echo sequence. As in the phantom imaging experiment images, the forward polarization mode, the reverse polarization mode and the color-coded images are shown from left to right. Figures were acquired using slice thicknesses of 5 mm, 20 mm, and without slice selection.
In the first row (gradient echo images with slice thickness of 5 mm and flip angle of 1^o), the catheter can be easily seen in the forward polarization mode image; background signal suppression was almost perfect in the reverse polarization mode image. On the other hand, with flip angle of 40^o, the catheter was barely visible in the forward polarization mode image, and background signal suppression was almost complete in the reverse polarization mode image. Color coding enabled visualization of both catheter and background.
As the slice thickness was increased (20 mm in Panel b, no slice selection in Panel c), visibility of the catheter decreased significantly in the forward polarization mode image even with a flip angle of 1^o. Identification of the catheter was almost impossible in the forward polarization mode image when a flip angle of 40^o was used. On the other hand, background suppression was effective in both reverse polarization mode images. Again, the color-coding method enabled visualization of the catheter against the background. (This figure was taken from [25])

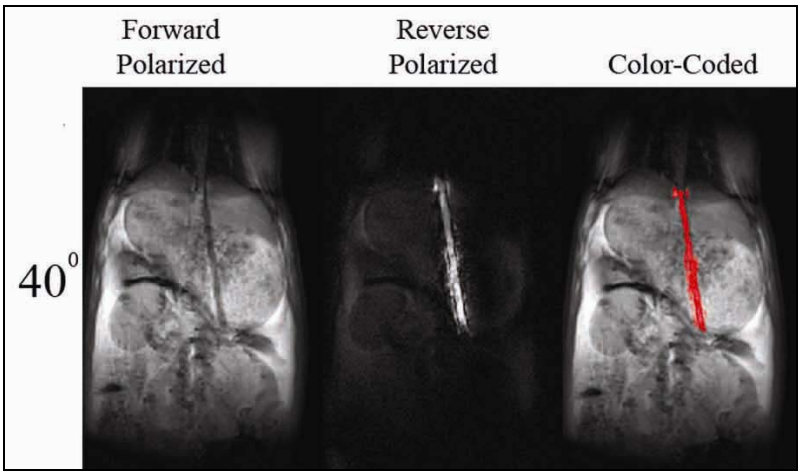

Figure 2.10: The animal imaging experiment with SSFP sequence. SSFP sequence is frequently used in guidance of interventional procedures. As expected, visibility of the catheter in SSFP sequence was low in the forward polarization mode image; on the other hand, background suppression in the reverse polarization mode image was successful. (This figure was taken from [25])

2.6. Discussion

A modified birdcage coil was manufactured in order to demonstrate the principles of the reverse polarization method. Our algorithm is very suitable for real-time implementation because it requires only one multiplication and one summation. Color-coding was already implemented in real-time [34].

The new method has not been implemented in a real-time imaging system. This will be essential if this method is to be useful in guiding interventional procedures. The processing power necessary to obtain reverse and forward polarization mode signals is minimal.

Our method can be used not only in catheter-tracking procedures but also possibly in tracking other interventional devices. For example, tracking coils [15] may be replaced by RCRF coils. This will eliminate the need for electrical connections between the interventional devices and scanner receivers [45], but needs further investigations.

In this study only phantom heat experiments were conducted. The exact conditions in which ICRF and RCRF coils can be used in MRI scanners needs to be investigated using detailed analysis backed by animal experiments and possibly with clinical tests. However, our results suggest that the heating around RCRF coils is significantly less than ICRF coils.

Currently, the use of implantable RF coils for high-resolution imaging of deep organs is under investigation [23]. One problem with the high-resolution imaging technique with implantable

coils is image overlaps. When a small field-of-view is used for high-resolution imaging, the large external coil receives signal from out of region of interest. This unwanted signal occasionally causes image overlaps. If a reverse polarization mode signal is used, the signal directly picked up by these coils can be eliminated and high-resolution imaging without image overlap may be possible.

This study started during my masters program and mentioned also in my Master's Thesis. However, most of the work was completed during my PhD program. Mainly, comparison of the ICRF and RCRF coils, phantom heating experiments, usage of the RCRF coil, all other imaging experiments were done after the completion of the MSc program.

2.7. Conclusion

The feasibility of background suppression using a reverse polarization mode signal in catheter tracking using inductively coupled RF coils was demonstrated. With a single birdcage coil, both reverse and forward polarization mode signals were obtained. Imaging of the target object with a real-time imaging sequence using the forward polarization mode signal was possible and the catheter was distinctly seen in the reverse polarization mode signal. Color-coding enabled simultaneous visualization of catheter and the anatomy without any restriction on the pulse sequence. The effectiveness of this method was tested by phantom and animal experiments. Clinical studies are needed to demonstrate the role of this technique in medicine.

3. REVERSE POLARIZED INDUCTIVE COUPLING TO TRANSMIT AND RECEIVE RF COIL ARRAYS

3.1. Introduction

In the previous chapter, the reverse polarization method for catheter tracking using a birdcage coil is introduced [25]. This method separates anatomical information from an RCRF. Although this method can be an excellent candidate for making the interventional devices visible, its main drawback is the requirement of a birdcage volume coil as the receiver. In today's practice birdcage coils are seldom used as receive coils because of their lower performance compared to the phased array coils [46]. Notably, it is known that individual simple elements of a phased array coil create a linearly polarized magnetic field [47], therefore it is not a trivial task to generate reverse polarized sensitivity using the phased array coils.

Here, a method is presented for obtaining reverse polarized sensitivity using a phased array coil system. It is also shown that by using duality, the proposed method can be employed to obtain reverse polarization through radio-frequency transmit-array systems.

"Wireless" active catheter tracking [32] and fiducial marker visualization [48-52] are demonstrated as applications of the proposed method. In both of these applications, induced radio-frequency current flows on a coupled RF (CRF) coil, amplifies the rotating magnetization vector, and finally turns into an oscillating magnetization in a linear path. This magnetization can be decomposed into rotating magnetization vectors, one travelling in the forward direction and the other in reverse. Since an anatomical signal can only be generated by the forward polarized magnetization vector, an image that is sensitive to the reverse polarized magnetization will solely contain the signal received by the CRF coil.

3.2. Theory

The reverse polarization method can be implemented using the receive and/or transmit paths.

3.2.1. Reverse Polarization Method Using Receive (Phased) Array RF Coils

As explained in the previous chapter, implementing the reverse polarization method to a receive coil with uniform sensitivity, such as the birdcage coil, is trivial because: i) both feeds of the birdcage coil have the same sensitivity magnitude, and ii) the phase difference between the feeds is same for all pixels. As a result, shifting the phase of the *y*-channel by -90^o or 90^o and summing with the *x*-channel produce forward or reverse polarized modes of the images [25, 53]. However, phased array coils do not have uniform sensitivity profiles and thus to obtain the reverse polarized mode of an image, a more sophisticated algorithm is necessary. In this section, the anatomy and CRF coil signals received by a linear phased array coil will be derived. In addition, the algorithm of the reverse polarization method for the receive array coils, which consist of linear coils, will be presented.

If the direction of the main magnetic field is reversed, a quadrature receive-only birdcage coil can not receive any MRI signal. On the other hand, if a linear coil, such as a simple loop coil, is used to receive the signal, the direction of the magnetic field is not important. In either case, the linear coil picks up the signal with equal sensitivity. When multiple linear coil elements are used as a phased array coil, their signals originating from the same point of interest can be combined to produce pure forward and reverse sensitivities. In the MR literature, the rotation direction of a magnetic field is usually explained in the rotating frame. Since both forward and reverse polarizations will be utilized in this study, it is difficult to explain this concept in the rotating frame. Therefore, in this text, magnetic fields will be expressed using the phasor notation with the $e^{i\omega_0 t}$ convention, where "i" is the imaginary unit number ($\sqrt{-1}$) and ω_0 is the Larmor frequency.

Assume that a phased array coil with *N* linear coil elements is used to image an anatomy with a CRF coil placed inside it. The phased array coil elements receive two types of signals from a point of interest close to the CRF coil: a direct signal of the spins and an indirect signal of the CRF coil. Rotating spins induce a current on the CRF coil and this current creates a linear

magnetic field that has both forward and reverse polarized components. The signal of the spins and then the signal of the CRF coil will be derived.

3.2.1.1. The anatomy Signal

Let $v_{n,anatomy}$ be the open circuit voltage of the n^{th} element of an *N*-channel phased array coil caused by the spins at the point of interest. In order to find the total voltage, this quantity needs to be integrated over the whole volume. However, by itself, this value is directly related to the sensitivity of the coil element at this point of interest. The voltage can be formulated using the reciprocity principle [54-56]:

$$v_{n,anatomy} = -i\omega_o \vec{M} \cdot \vec{B}_n \text{,} \tag{3.1}$$

where "$\cdot$", represents the dot product and $\vec{M}$ is the phasor representation of the rotating magnetization vector given by:

$$\vec{M} = m\left(\hat{a}_x + i\hat{a}_y\right) \tag{3.2}$$

where *m* is the complex representation of the transverse magnetization and, $\hat{a}_x$ and $\hat{a}_y$ are unit vectors in x and y directions, respectively.

Note that Eq.(3.2) is the phasor equivalent of the time domain representation of the magnetization $\vec{M}(t) = |m|\cos(\omega_0 t + \angle m)\hat{a}_x - |m|\sin(\omega_0 t + \angle m)\hat{a}_y$. In Eq.(3.1), $\vec{B}_n$ is the magnetic field at the point of interest generated by the n^{th} element of the receive phased array coil when a unit current is applied to the terminals of the coil element (Figure 3.1a). Note that $\vec{B}_n$ is a linearly polarized magnetic field and all the elements of the phased array coil have the same phase at a point of interest since this value is carefully calibrated in the MRI scanner. In this study, the *z*-component of the magnetic field is ignored since it has no contribution to this analysis.

3.2.1.2 CRF Coil Signal

The CRF coil is the secondary source of the magnetic field, i.e. the spins around the CRF coil induce the current, I_{CRF}, on the CRF coil. This current on the small CRF coil can be represented by a magnetization oscillating on a linear trajectory (Figure 3.1b).

Note that a linearly polarized magnetization can be decomposed into two counter-rotating magnetizations, i.e. the forward and reverse polarized magnetizations. The linearly polarized external receive coils are sensitive to both components of the linearly polarized magnetization.

Similar to the anatomy case in Eq.(3.1), the voltage induced on the n^{th} coil by the CRF coil can be expressed using the magnetization vector of the CRF coil, $\vec{M}_{CRF}$, as (Figure 3.1b):

$$v_{n,CRF} = -i\omega_o \vec{M}_{CRF} \cdot \vec{B}_n . \tag{3.3}$$

Note that the magnetic field, $\vec{B}_n$, is assumed to be the same magnetic field as in Eq.(3.1), because the CRF coil is small and the point of interest is very close to it. The magnetization of the CRF coil originates from the current and is proportional to its unit surface area, *s*, and the normal vector:

$$\begin{aligned} \vec{M}_{CRF} &= I_{CRF}\, s \left(\cos\theta\, \hat{a}_x + \sin\theta\, \hat{a}_y\right) \\ &= I_{CRF}\, s \left[e^{i\theta} \left(\hat{a}_x - i\hat{a}_y\right) + e^{-i\theta} \left(\hat{a}_x + i\hat{a}_y\right) \right] \Big/ 2 \end{aligned} \tag{3.4}$$

Above, θ is the orientation angle of the CRF coil with respect to the *x*-axis.

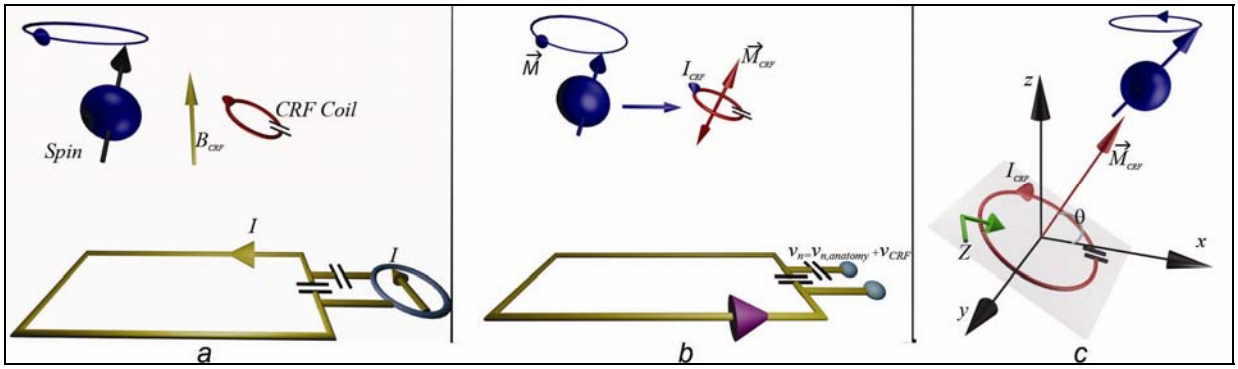

Figure 3.1: Sketch of the n^{th} element of the phased array coil, CRF coil, and spin interactions. a) $\vec{B}_n$ is the magnetic field generated by the n^{th} element of the receive phased array coil at the point of interest when the unit current, *I*, is applied to the terminals of the coil element. b) $\vec{M}$ is the rotating magnetization vector of spins and $\vec{M}_{CRF}$ is the magnetization vector of the CRF coil that is oscillating in a linear trajectory. The spins around the CRF coil induce a current, I_{CRF}. This current on the small CRF coil can be represented by a magnetization vector, $\vec{M}_{CRF}$. As a result of these magnetizations, a voltage, v_n, is induced on the terminals of the external coil. c) $\vec{B}_c$ is the magnetic field generated by the CRF coil at a point of interest when a unit current, *I*, is applied to an imaginary terminal of the coil. θ is the orientation angle of the w.r.t x-axis of the CRF coil, and *Z* is the impedance at this imaginary terminal of the CRF coil.

Here, an important property of the CRF coil is that its magnetization vector can be decomposed into forward and reverse polarized components of equal magnitude:

$$\vec{M}_{CRF} = \vec{M}_{CRF,f} + \vec{M}_{CRF,r}, \tag{3.5}$$

where

$$\begin{aligned} \vec{M}_{CRF,f} &= s\, I_{CRF}\, e^{-i\theta} \left(\hat{a}_x + i\hat{a}_y\right)/2 \\ \vec{M}_{CRF,r} &= s\, I_{CRF}\, e^{i\theta} \left(\hat{a}_x - i\hat{a}_y\right)/2 \end{aligned} \tag{3.6}$$

Integrating Eq. (2.5) into Eq. (2.3) results in:

$$v_{n,CRF} = -i\omega_o \left\{ \left[\vec{M}_{CRF,f} + \vec{M}_{CRF,r} \right] \cdot \vec{B}_n \right\}. \tag{3.7}$$

The induced current on the CRF coil can be calculated using a method similar to the derivation of the anatomy signal. The main difference is that the CRF coil has no terminal; therefore the induced current is calculated instead of the voltage. Assume that $\vec{B}_c$ is the magnetic field generated by the CRF coil at a point of interest when a unit current is applied to an imaginary terminal of the coil (Figure 3.1b); then the induced current on the CRF coil due to the magnetic resonance phenomenon is:

$$I_{CRF} = -i\,\omega_o\, m\, B_c e^{i\theta} / Z, \tag{3.8}$$

where Z is the impedance at this imaginary terminal (Figure 3.1c). As a result, $v_{n,CRF}$ can be expressed in terms of $v_{n,anatomy}$:

$$v_{n,CRF} = m\, S_n\, c_f + m\, S_n^*\, c_r, \tag{3.9}$$

where S_n is the sensitivity of the n^{th} element and defined as $S_n = v_{n,anatomy} / m$. Here, "*" is the conjugation operator and c_f and c_r are the forward and reverse polarization amplification factors, respectively:

$$c_f = -i\,\omega_o\, s\, B_c / 2Z$$
$$c_r = i\,\omega_o\, s\, e^{i2\theta} e^{i2\phi} B_c / 2Z \tag{3.10}$$

Note that there is only a phase difference between these values.

Finally, the total voltage can be expressed by the sum of the anatomy and CRF coil voltages:

$$\begin{aligned} v_n &= v_{n,anatomy} + v_{n,CRF} \\ &= S_n \left(m\, c_f + m \right) + S_n^*\, m\, c_r \end{aligned} \tag{3.11}$$

As a result, the matrix form of the above equation is:

$$\begin{bmatrix} v_1 \\ v_2 \\ \vdots \\ v_N \end{bmatrix} = \begin{bmatrix} S_1 & S_1^* \\ S_2 & S_2^* \\ \vdots & \vdots \\ S_N & S_N^* \end{bmatrix} \begin{bmatrix} m + m\, c_f \\ m\, c_r \end{bmatrix}. \tag{3.12}$$

3.2.1.3. The Reverse Polarization Algorithm

This chapter of the dissertation deals with the challenge of extracting the reverse polarization component of a signal $m\,c_r$ from the acquired data. By doing this, a coupled coil placed on a catheter or on a body as a fiducial marker can be identified.

The vector on the left-hand side of the above equation is already known and represents pixel values on the images that are reconstructed using the signal received by each of the coil elements. In order to find $m\,c_r$, the sensitivity values for each coil element must be known. Once the sensitivities of all coil elements are known, the reverse polarized component of the signal (together with the forward component as a byproduct) can be obtained by a matrix pseudo-inversion operation:

$$\begin{bmatrix} m + m\, c_f \\ m\, c_r \end{bmatrix} = \begin{bmatrix} S_1 & S_1^* \\ S_2 & S_2^* \\ \vdots & \vdots \\ S_N & S_N^* \end{bmatrix}^{\dagger} \begin{bmatrix} v_1 \\ v_2 \\ \vdots \\ v_N \end{bmatrix} \tag{3.13}$$

where "†" represents a pseudo-inversion operator.

3.2.2. Reverse Polarization Method Using Transmit Array Coils

The algorithm of the reverse polarization method for the receive array coils is explained above. To tackle this problem, the reverse polarized signal needs to be calculated for each pixel of the image using a post-processing algorithm. Using the reciprocity principle, one can conclude that the reverse polarization algorithm for the transmit array is a dual problem. Unlike the receive arrays, the transmit operation cannot be conducted using post-processing. Therefore, by using the above algorithm, reverse polarization can only be achieved on a single point in space. In order to solve this issue, the algorithm can be generalized for multiple points, but the formulation indicates that reverse polarization can be obtained on only *N/2* points with an *N*-channel transmit array system. By properly distributing these points in a region of interest, one may obtain reverse polarization in that region.

Alternatively, a birdcage coil may be fed from its two quadrature ports independently as a transmit array coil. In this configuration, obtaining reverse polarized transmission is straightforward [25]. Shifting the phase of the *y*-channel by -90^{o} or 90^{o} with respect to the *x*-channel produces forward or reverse polarized excitation modes. A radio-frequency magnetic field does not excite spins if it is rotating in the "reverse" direction, but it induces a current on the CRF coil. Then, the secondary field created by the CRF coil excites spins in its vicinity. Therefore, when reverse polarized excitation is used, the anatomy signal will be suppressed and consequently the reconstructed image will consist of the CRF signal only.

Note that with the help of the transmit array system, both forward and reverse (or linear) excitations are possible, and the forward or reverse polarization mode of an image can be obtained without post-processing.

3.3. Method

In this study, a three-tesla Siemens TIMTrio with an experimental eight-channel transmit array system was used. Siemens body, spine, and head matrix coils were used for signal reception.

These coils use mode matrix combiners [57] and destruct the linear polarization data of the coil elements. In order to reconstruct the linear polarized data, mages were acquired in triple mode and proper complex constants were multiplied with the element data and recombined. A MATLAB code was written for this purpose.

The coil sensitivity information is crucially important for the reverse polarization method. The sensitivity maps can be acquired using different methods [58-61]. In this study, these maps were obtained using the central part of the k-space matrix or spatial low-pass filtering. The filtering removes the effect of the CRF coil on the image because the coil is small and its information is in the high-frequency components of the image However, one cannot obtain CRF data by high-pass filtering because the anatomy also has high-frequency components. The sensitivity map window, which determines the area at the center of the k-space matrix, was adjusted according to the applications.

After obtaining the sensitivity maps, the reverse polarization factor for each pixel was calculated using the pseudo-inverse command "pinv" of MATLAB. The reverse polarization mode of the image was color-coded and combined with the squared-summed image of the subject.

The transmit array system on site has eight RF channels and their relative phases must be calibrated before the experiments as they change after each system reboot. By using the reverse polarization mode, two transmit channels were calibrated, i.e. the phase was adjusted to obtain the noisy reverse polarization mode of the image. In the ideal case, adding 90^{o} to the *y*-channel and running both channels create the reverse polarized field and no spins are excited. Because of the shift caused by the system reboot, the *y*-channel phase was scanned between 40^{o} to 140^{o} with an increment of 10^{o}. The image with a minimum signal level was assumed to be the reverse polarized mode of the image. After fine tuning, the relative phase between the *x*- and *y*-channels was found.

The proposed method was implemented for both catheter tracking and fiducial marker visualization applications.

3.3.1. Catheter Tracking

The ICRF coil was 100 mm long and constructed on a 6 F Teflon catheter using a coated copper wire 0.4 mm in diameter. A heat shrink tube was used for isolation, resulting in a prototype device with an outer diameter of 3 mm (3 french is 1 mm) (Figure 3.2). It was tuned by a 22 pF ceramic chip capacitor to 123.23 MHz using an HP 8753D network analyzer. A pair of back-to-back MMBD7000LT1 switching diodes in parallel to the 22 pF tuning capacitors was used for the decoupling of the RCRF coils.

In the phantom experiments, images were acquired using the spine and body matrix phased array coils in both the transmit and receive array experiments, and fast gradient echo with the following imaging protocol: TR/TE: 40/3.4 ms, flip angle: 40^0, slice thickness: 5 mm, FOV: 20 cm, matrix: 256 X 256.

3.3.2. Fiducial Marker Visualization

The ICRF coil was constructed with three turns of copper wire of 0.5 mm in diameter, forming a circle with a diameter of 5 mm (Figure 3.3). It was tuned by a 16 pF ceramic chip capacitor to 123.23 MHz using an HP 8753D network analyzer. In both the transmit and receive array phantom experiments, images were acquired using the head matrix phased array coil and fast gradient echo with the following imaging protocol: TR/TE: 40/3.4 ms, flip angle: 40^0, slice thickness: 5 mm, FOV: 20 cm, matrix: 256 X 256. A Siemens sodium chloride (NaCl) solution

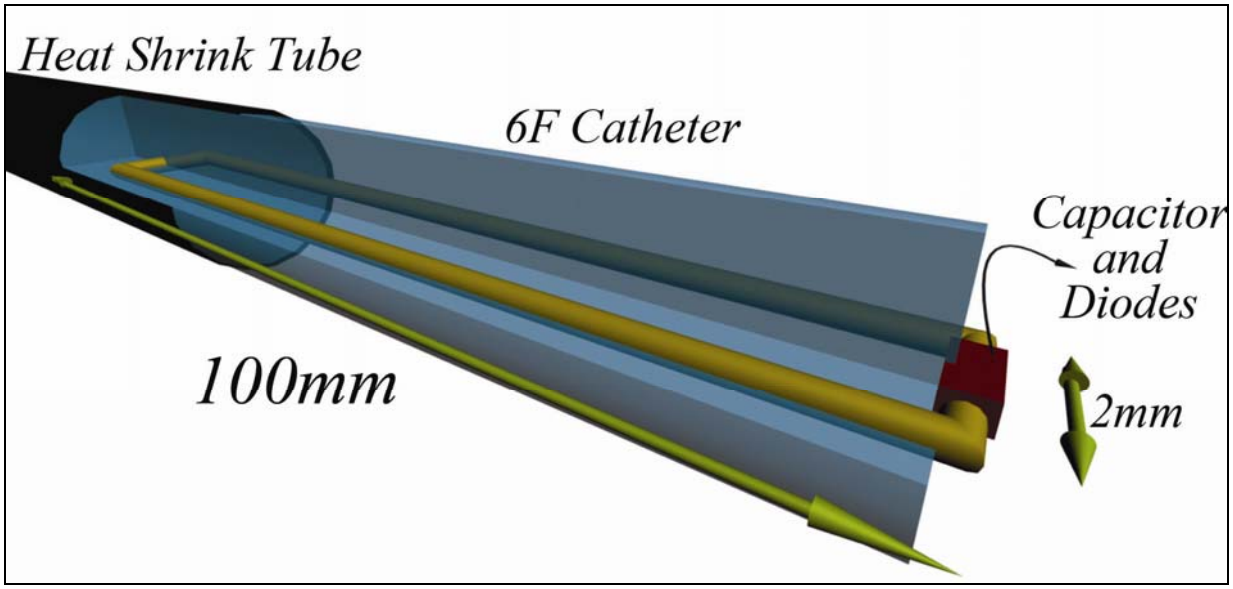

Figure 3.2: The CRF coil design.

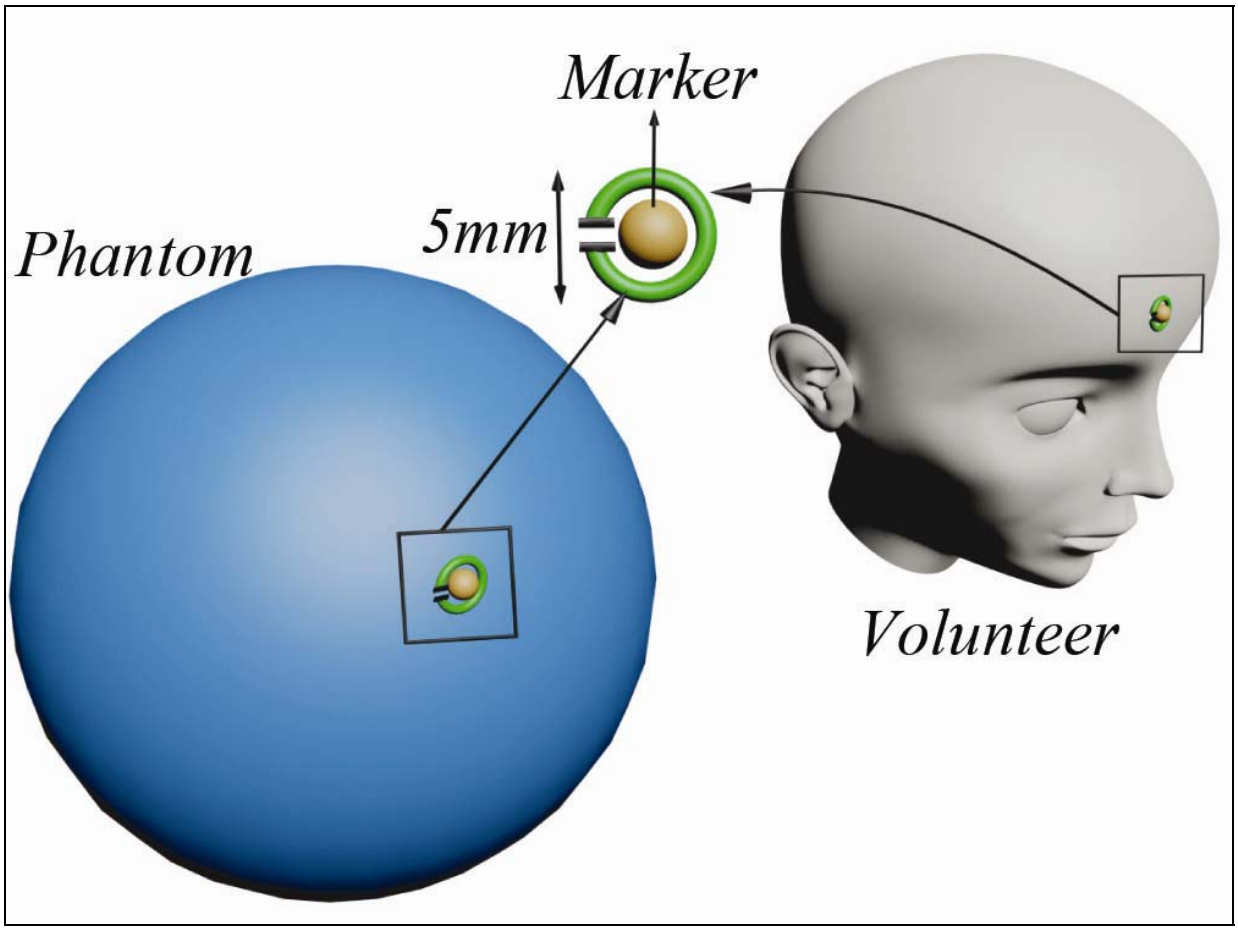

Figure 3.3: Sketch of the NaCl solution phantom and a volunteer for fiducial marker visualization.

phantom was used in phantom experiments. The same ICRF coil and experiment setup were used in the volunteer experiments. The experiments conformed to the Guidelines for Experiments with Human Participants, and were approved by the Bilkent University ethics committee, Ankara, Turkey.

3.4. Results

3.4.1. Catheter Tracking:

3.4.1.1. Receive Array

Figure 3.4 shows the oblique images of an oil phantom with two straws, one filled with KCl solution and the other with an RCRF coil inside. Figure 3.4a is the forward polarization mode of the image, Figure 3.4b is the reverse polarization mode of the image, and Figure 3.4c the color-coded image. Although there is a KCl solution-filled straw as a disturber, the reverse polarization method can separate the RCRF coil from the phantom.

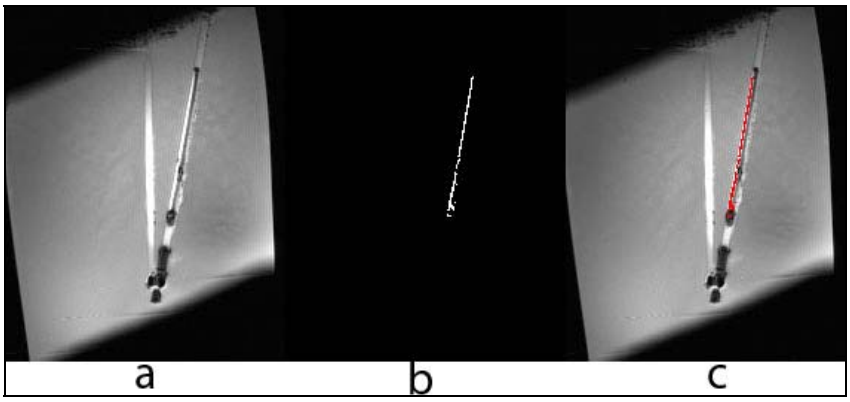

Figure 3.4: Oblique images of the phantom. (a) The forward polarization mode of the image, (b) the reverse polarization mode of the image, and (c) the color-coded image.

The results prove that the reverse polarization algorithm successfully suppresses both oil and contrast agent signals with receive (phased) array coils.

3.4.1.2. Transmit Array

Figure 3.5 shows a sagittal image of an oil phantom with two straws, one filled with KCl solution and the other with an ICRF coil inside. Figure 3.5a shows the forward polarization mode of the image, Figure 3.5b is the reverse polarization mode of the image, and Figure 3.5c is the color-coded image. Although the phantom and contrast agent signals are stronger than the ICRF coil signal (left column), the reverse polarization method using the transmit array system suppresses all the signals other than the linearly polarized signal of the ICRF coil.

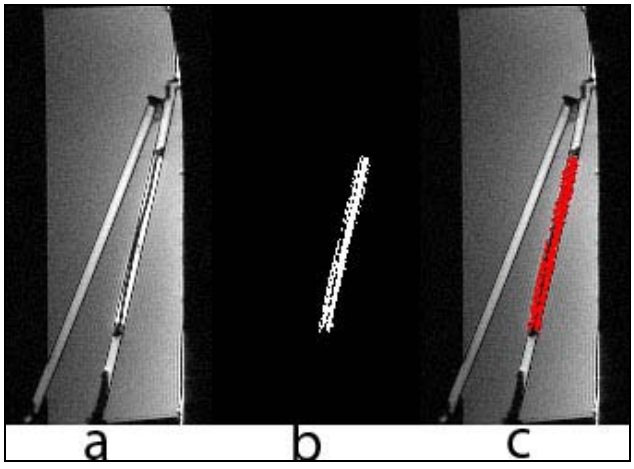

Figure 3.5: Sagittal images of the phantom and ICRF coils. (a) The forward polarization mode of the image, (b) the reverse polarization mode of the image, and (c) the color-coded image.

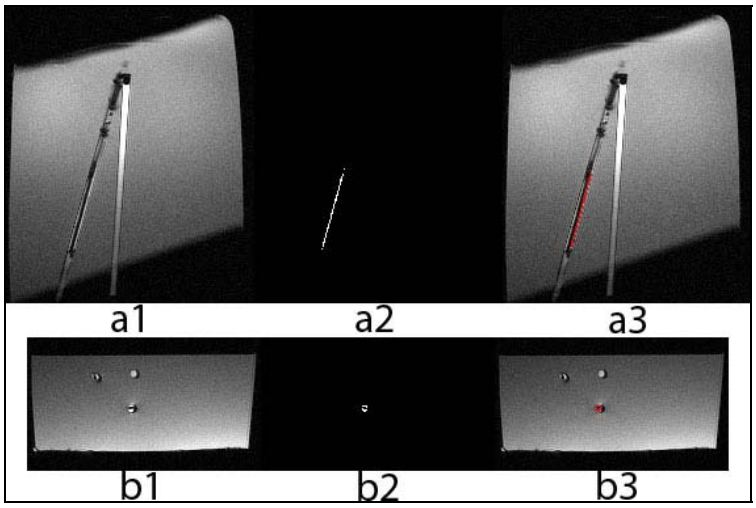

Figure 3.6: a) Oblique images of the phantom and ICRF coils. (a1) The forward polarization mode of the image, (a2) the reverse polarization mode of the image, and (a3) the color-coded image. Similar to the previous case shown in Figure 3.5, the method successfully singles out the RCRF coil signal. However, because of the transmission decoupling, the RCRF signal is weaker than the ICRF coil signal. b) Transversal images of the ICRF coil, RCRF coil, and KCl solution. (b1) The forward polarization mode of the image, (b2) the reverse polarization mode of the image, and (b3) the color-coded image. Although the phantom and contrast agent signals are stronger than the ICRF coil signal (left column), the reverse polarization method using the transmit array system suppresses all signals other than the linearly polarized signal of the ICRF coil.

The results shows that the transmit array system enables the suppression of the anatomy signal. Next, the RCRF coil is used with the transmit array system. As shown in Figure 3.6a, the catheter still appears bright, suggesting flip angle amplification. This can be explained by the fact that the voltage across the diodes is the turn-on voltage and a small amount of current flows through the RCRF coil.

Figure 3.6b shows a transversal image of three straws, first filled with KCl solution, second with an ICRF coil inside and third with an RCRF coil. Both the anatomy and RCRF signals are suppressed when the reverse polarization method was applied to the transmit array system while the ICRF coil image was reconstructed.

3.4.2. Fiducial Marker Visualization:

3.4.2.1. Phantom Experiments:

Figure 3.7a shows sagittal images of a saline solution phantom with an ICRF coil attached to the phantom (Figure 3.3). The reverse polarization algorithm successfully suppresses both oil and contrast agent signals with receive (phased) array coils. The color-coded images show that the algorithm works.

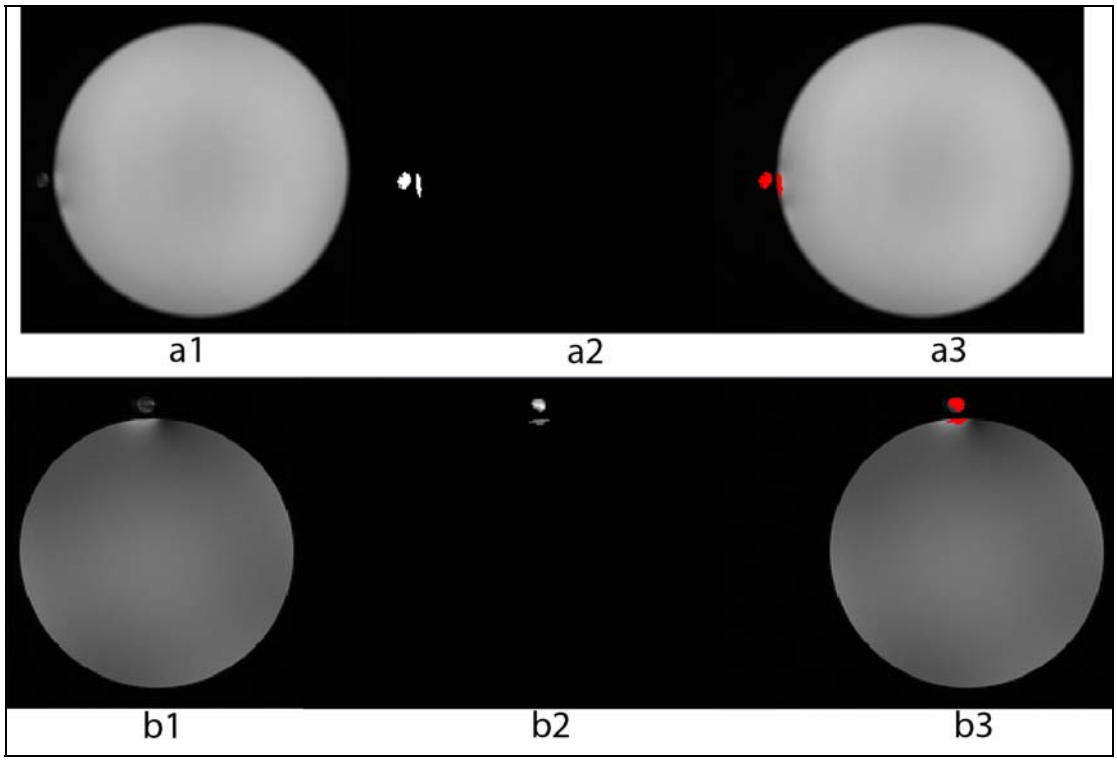

Figure 3.7: a) Oblique image of the receive array. (a1) The forward polarization mode of the image, (a2) the reverse polarization mode of image, and (a3) the color-coded image.
b) Oblique image of the transmit array. (b1) The forward polarization mode of the image, (b2) the reverse polarization mode of the image, and (b3) the color-coded image. Similar to the receive array case, suppression of the anatomy signal for MR guidance is effective.

3.4.2.2. Volunteer Experiments:

Volunteer experiments are especially important to show the usefulness of the reverse polarization method for clinical applications. The transversal and sagittal images are shown in Figures 3.8 and 3.9 respectively. All figures presented in this section show that the reverse polarization method works successfully in both applications. The background signal is almost completely suppressed and the color-coded images enable visualization of the CRF coils.

3.5. Discussion

As already known, the forward polarized transmission excites spins and coupled RF (CRF) coils whereas the reverse polarized transmission excites only CRF coils. With conventional imaging systems, only forward or reverse polarized transmission is possible. Transmit array systems, however, can switch between forward and reverse polarizations simultaneously. Transmit array studies are mostly concentrated on homogenizing higher frequency RF fields, but this causes another problem, namely excessive specific absorption rate (SAR). In this study, the transmit and receive (phased) arrays offer separate excitation and reception profiles

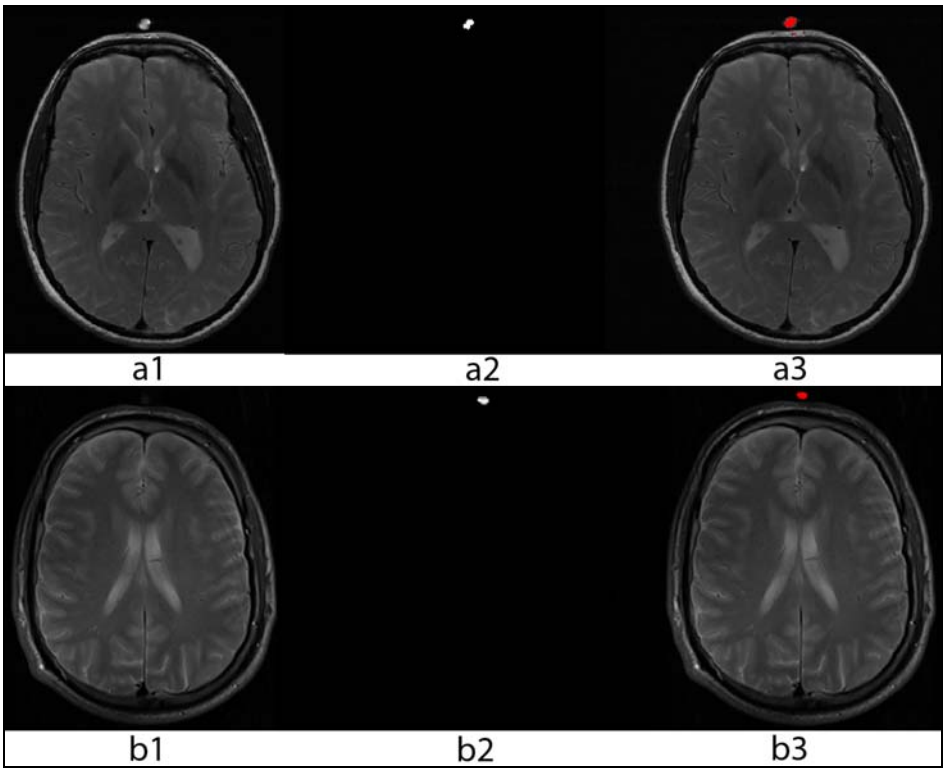

Figure 3.8: a) Transversal image of receive array coil. (a1) The forward polarization mode of the image (a2), the reverse polarization mode of the image, and (a3) the color-coded image.
b) Transversal image of transmit array. (b1) The forward polarization mode of the image, (b2) the reverse polarization mode of the image, and (b3) the color-coded image.
It is already embedded in the imager and because it uses only two channels, it is simpler to work with.

in order to improve the usability of the reverse polarization method. Here, the receive array coil data was processed to obtain a reverse polarization mode image and the transmit array system was utilized to excite the CRF coil only, suppressing the anatomy signal. In this study we used the Siemens' experimental 8-channel transmit array system. The applications discussed in this paper use only two channels and the phases and amplitudes of the RF waveforms are manipulated but the shape of the waveforms were identical. Although the transmit array system's capabilities are not completely utilized, the body coil is much more accessible.

In this study, the reverse polarization method was also implemented in fiducial marker visualization. During an invasive operation, a targeting procedure is vital. Fiducial markers are effectively used in different operations for registration purposes. However, in some sequences, these markers are not bright enough, so registering becomes more difficult. In order to improve the visibility of the markers, the reverse polarization method was implemented using CRF coils for image-guided surgery registration.

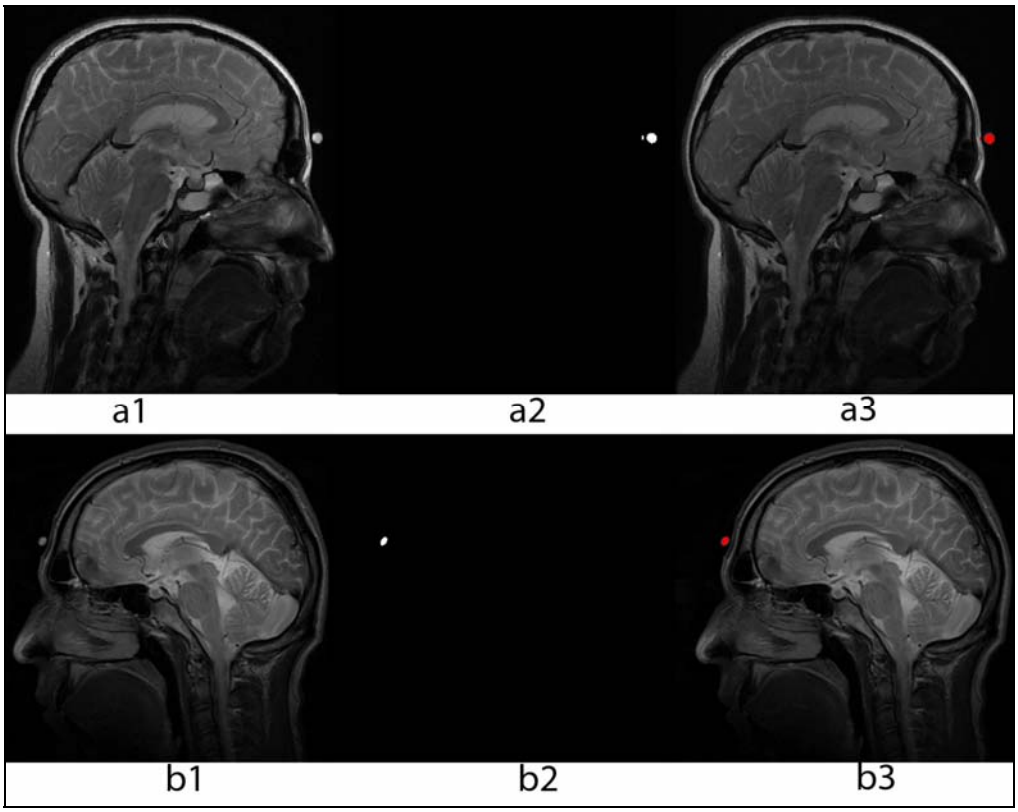

Figure 3.9: a) Sagittal image of receive array coil. (a1) The forward polarization mode of the image (a2), the reverse polarization mode of the image, and (a3) the color-coded image. b) Sagittal image of transmit array. (b1) The forward polarization mode of the image, (b2) the reverse polarization mode of the image, and (b3) the color-coded image.

Lastly, it should be mentioned that oil was used in the phantom experiments, which helped avoid dielectric effect-related inhomogeneities [62]. Furthermore, the *x*-channel of the body coil was performing significantly worse than the *y*-channel. In order to obtain the same signal strength from individual channels separately, the *y*-channel was multiplied by 0.67, while the multiplier of the *x*-channel was kept at 1.00. Our initial tests on human volunteers did produce enough homogeneity while using our 3 tesla scanner so that we were able to demonstrate the method in vivo.

3.6. Conclusion

The feasibility of the reverse polarization method was examined using transmit and receive array systems in two different applications of the method, i.e. catheter tracking and fiducial marker visualization. Using both transmit and receive RF coil arrays coupled to RCRF and ICRF coils, we showed that the method achieved successful background suppression in both phantom and volunteer studies.

4. TRACKING ROTATIONAL ORIENTATION AND POSITION OF CATHETER USING TRANSMIT ARRAY SYSTEM

4.1. Introduction

A precise and fast localization of interventional devices is a necessity in order to perform minimally invasive operations. Generally, X-ray is used for these operations due to almost perfect instrument visualization and determination of catheter orientation. However, X-ray cannot provide soft tissue contrast and ionizing radiation is exposed to patients as well as staffs. On the other hand, MRI is a non-ionizing imaging modality that offers impressive soft tissue contrast as compared to X-ray. One of the main challenging problems in MR-guided interventions is the difficulty in real-time detection and tracking of the interventional devices. Various techniques have been developed for identification of interventional devices. Although, the passive and active catheter tracking methods have distinct advantages, the passive tracking methods have reliability problems [9], and device handling in the active tracking techniques (2-4) is uneasy. There are also hybrid methods which make use of an ICRF [21, 25] coil. Even though many researchers tried to deal with the tracking problem, only Anderson et al. addressed a solution for the rotational orientation issue using phase images of active micro coils manually [26].

In all of the applications and methods mentioned above, conventional imaging systems have been used. On the other hand transmit array systems have recently been introduced for experimental studies. Yet these studies are mostly concentrated on understanding the working principles, exploring the capabilities of the system, and homogenizing the high frequency B_1 fields [63-65]. Although usage of transmit array systems has been limited, the use of transmit

array system was introduced in the previous chapter in order to obtain reverse polarization during transmission.

In this study, a new method that uses a transmit array system is presented in order to i) detect rotational orientation and ii) track position of interventional devices on which ICRF coils are constructed.

The method enables simultaneous acquisition of anatomy and ICRF coil images using the FLASH (Fast Low Angle SHot Magnetic Resonance Imaging) [66] and TrueFISP (True fast imaging with steady state precession) [67] sequences. Both FLASH and TrueFISP sequences are fast and therefore used in real time applications. Furthermore, this method paves the way of using asymmetric designs of the catheter, because the rotational orientation information increases the control on the catheter and it can be useful for several applications, such as MR-guided intravascular focused ultrasound (IVUS) [27, 28] with independent transducer arrays [29] and RF ablation.

4.2. Theory

In this study, conventional RF excitation pulses are modified and a transmit array system is used to apply to the transmit coil. The anatomy and ICRF coil signals due to the new RF pulse scheme will be derived analytically in this section.

4.2.1. Conventional Body Coil Excitation

As mentioned in earlier chapters, a body birdcage coil has two feed points and conventionally, a quadrature hybrid is used to deliver the excitation signal through a single channel. [25, 53]. The quadrature hybrid divides the signal into two halves with the same magnitude and 90^{o} phase difference (Figure 4.1). This generates forward polarized RF field [25]. The conventional excitations use identical RF pulses with constant amplitude in each TR. Typically a body birdcage coil is used to generate the forward polarized RF excitation (Figure 4.1). This rotational excitation is two times better in total body SAR and four times better in peak SAR than linear excitation, because all power is delivered to the subject.

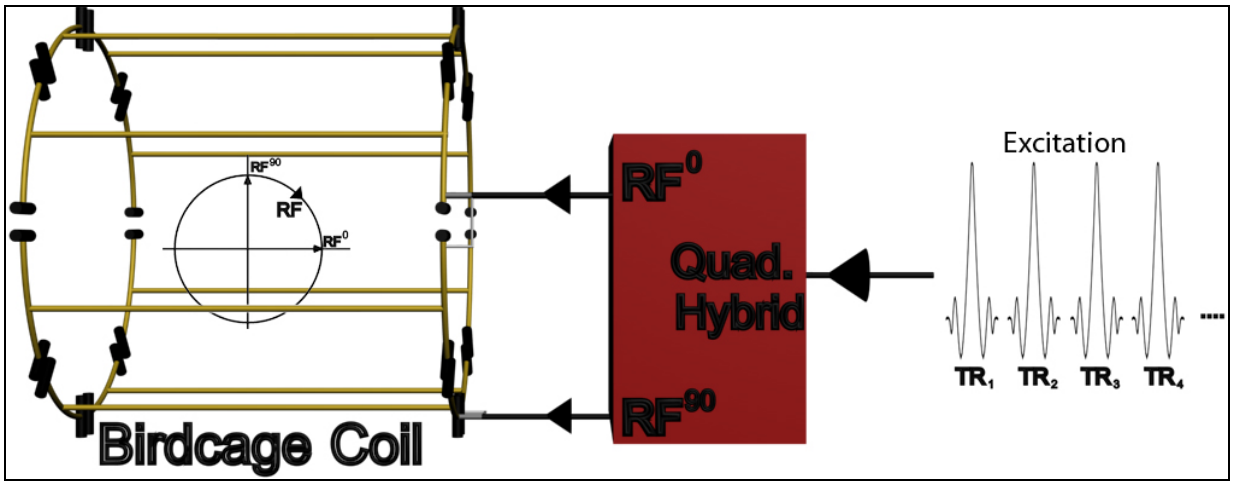

Figure 4.1: A conventional MRI RF excitation and the field polarization using a single channel body birdcage coil with a quadrature hybrid. The quadrature hybrid divides input excitation signal into two halves with 90° phase difference. This excitation enables a forward polarized field inside a birdcage coil.

4.2.2. Transmit Array Excitation

Assume a body birdcage coil is used as a two channel transmit coil by eliminating the quadrature hybrid. If the same RF excitation mentioned in Figure 4.1is applied to the both feeds of the transmit birdcage body coil, a linearly polarized RF excitation is obtained with 45° angle with respect to x-axis (Figure 4.1).

Assuming the spin magnetization in the anatomy is given by $M_{T,Anatomy}$, the anatomy signal can be expressed as:

$$S_{Anatomy}(t) = \iint \left(M_{T,Anatomy}\, e^{i\pi/4} \right) e^{-i2\pi k_x x} e^{-i2\pi k_y} dx\, dy \qquad (4.1)$$

Eq. (4.1) states that an image similar to the original image which is the result of Figure 4.1 is reconstructed at the same location with 45° phase, but this phase does not effect the reconstructed image. Note that k_x and k_y are functions of time. Assume S is the k-space matrix of an arbitrary object that is the result of the sequence (Figure 4.2) and S_{TRp} is the k-space row result of the p^{th} TR.

In this study, a modified design of RF excitations with turning linear polarization vector is used. The circulation is done by changing the direction of the linear polarization in each TR.

As an example, consider the RF excitation scheme shown in Figure 4.3. In this design, the RF excitation amplitudes are changed to obtain a circulation that progress $\pi/2$ in each TR.

As the RF pulse scheme changes, the complex transverse magnetization of the anatomy changes. One can generalize the magnetization of the p^{th} RF (or p^{th} TR) as:

$$M^{+}_{nT,Anatomy}(t) = M_{T,Anatomy}\, e^{ip\pi/2} \tag{4.2}$$

The above equation states that, each row of the S matrix is multiplied by a complex factor, which is the phase of the RF_{TRp}.

As a result, signal can be expressed as:

$$S_{Anatomy}(t) = \iint \left(M_{T,Anatomy}\, e^{ip\pi/2} \right) e^{-i2\pi\left(k_x x + k_y y\right)} dx\, dy \tag{4.3}$$

where k_x and k_y are spatial frequency variables in x and y directions respectively. Assuming y as the phase encoding direction, p can be expressed in terms of imaging parameters as:

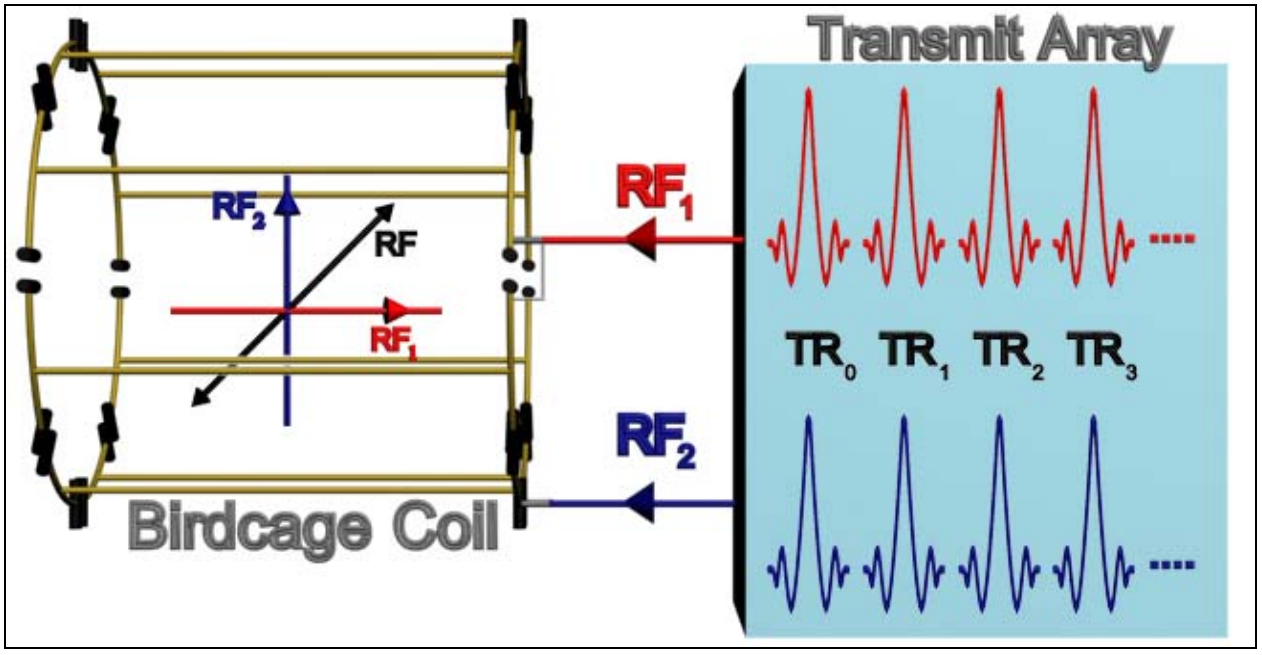

Figure 4.2: Standard spoiled GRE sequence RF pulse schemes and the birdcage coil excitation using the transmit array system. If the quadrature hybrid is eliminated and two excitation channels are input with a same spoiled GRE excitation pulses a linearly polarized field is created inside the birdcage coil.

$$p = k_y N_y \Delta y \tag{4.4}$$

where N_y is the number of phase encoding lines, and Δy is the image resolution in phase direction. Substituting Eq. (4.4) into Eq. (4.3) gives:

$$S_{Anatomy}(t) = \iint \left(M_{T,Anatomy}\, e^{-i2\pi k_x x} e^{-i2\pi k_y \left(y - N_y \Delta y/4\right)} \right) dx\, dy \tag{4.5}$$

which means the perturbation due to modified RF excitation causes a shift of the image location in phase direction with an amount of $2N_y/P$, where P is the number of RF pulses in one turn, in above example, $P = 4$.

On the other hand, the magnetic field created by the ICRF coil is directly related to orientation of itself. Therefore, the complex transverse magnetization of the ICRF coil has to be derived in a more detailed manner.

4.2.2.1 ICRF Coil Magnetization

The effect of the turning linear polarization vector to the ICRF coil is different than the

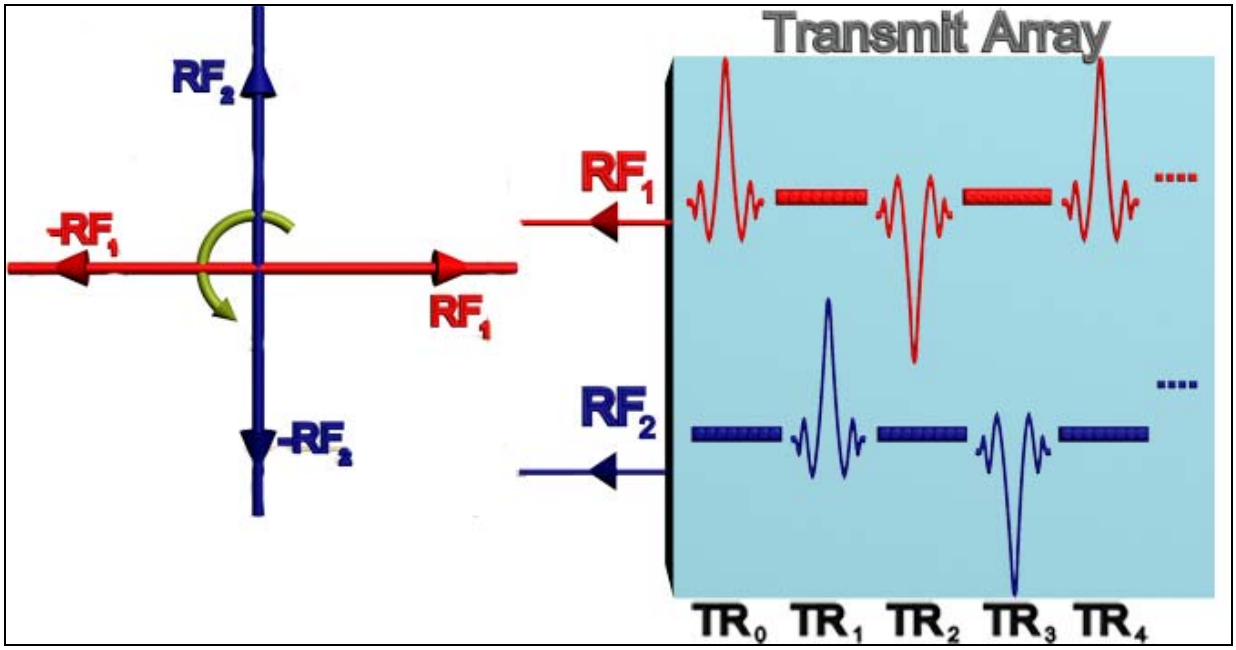

Figure 4.3: The modified RF excitation scheme and the birdcage coil field using the transmit array system. Excitations of the channels change such that a linearly polarized field with a turning polarization vector is created.

anatomy case. In the previous case, change in the RF direction only causes phase change in the k-space. However, in order to explore the constants that are multiplied by the k-space lines, one has to take the orientation dependence of the ICRF coil into account. If the ICRF coil is not decoupled from the transmit field by a pair of back-to-back diode, the transmit field induces current on the ICRF coil. The induced current creates a secondary the magnetic field. This time dependent magnetic field created by the ICRF coil can be represented as:

$$\vec{B}_{ICRF,t}(t) = I_{ICRF,t}(t)\vec{B}'_{ICRF} \tag{4.6}$$

where $I_{ICRF,t}(t)$ is the time dependent current due to transmit field:

$$I_{ICRF,t}(t) = B_t(t)\cos(\omega_o t + \sigma)\hat{a}_t \cdot \vec{s} \tag{4.7}$$

where $B_t(t)$ is time dependent peak value of transmit magnetic field, ω_o is the Larmor frequency, σ and $\hat{a}_t$ are the phase and unit vector of $B_t(t)$ **,** and $\vec{s}$ is surface normal vector of the ICRF coil, given by:

$$\vec{s} = s\left(\cos\theta\,\hat{a}_x + \sin\theta\,\hat{a}_y\right) \tag{4.8}$$

where s is the area of the ICRF coil and θ is the orientation of the ICRF coil with respect to *x*-axis. For every different RF pulse mentioned in Figure 4.3, dot product of the surface normal vector of the ICRF coil and the unit vector of the transmit magnetic field (Eq. (4.7)) causes different complex parameter.

In Eq. (4.6), $\vec{B}'_{ICRF}$ is the peak value of magnetic field generated by the ICRF coil at a point of interest when a unit current is applied to an imaginary terminal of the coil:

$$\vec{B}'_{ICRF} = B_{co}\left(\cos(\theta+\eta)\hat{a}_x + \sin(\theta+\eta)\hat{a}_y\right) \tag{4.9}$$

where B_{co} is the magnitude of the magnetic field, $\theta+\eta$ is the orientation of the magnetic field vector at the point of interest, η is the phase term of the magnetic field related to other than the orientation of the ICRF coil. Note that, the field vector orientation is directly related to the orientation of the ICRF coil, therefore θ appears in the magnetic field expression. Using above equations, *x* and *y* components of the $\vec{B}_{ICRF,t}(t)$ can be expressed as:

$$\begin{aligned} B_{ICRF,tx}(t) &= B_t(t)\,B_{co}\,s\left[\hat{a}_t\cdot\left(\cos\theta\,\hat{a}_x+\sin\theta\,\hat{a}_y\right)\right]\cos\left(\omega_o t+\sigma\right)\cos\left(\theta+\eta\right) \\ B_{ICRF,ty}(t) &= B_t(t)\,B_{co}\,s\left[\hat{a}_t\cdot\left(\cos\theta\,\hat{a}_x+\sin\theta\,\hat{a}_y\right)\right]\cos\left(\omega_o t+\sigma\right)\sin\left(\theta+\eta\right) \end{aligned} \tag{4.10}$$

Converting the lab frame expressions into the rotating frame will be useful for calculations. Using rotation matrix:

$$\begin{aligned} B_x^+(t) &= B_{ICRF,tx}(t)\cos\left(\omega_o t\right)+B_{ICRF,ty}(t)\sin\left(\omega_o t\right) \\ B_y^+(t) &= -B_{ICRF,tx}(t)\sin\left(\omega_o t\right)+B_{ICRF,ty}(t)\cos\left(\omega_o t\right) \end{aligned} \tag{4.11}$$

where $B_x^+(t)$ and $B_y^+(t)$ are the *x* and *y* components of the positively rotating frame [54]. Ignoring $2\omega_o t$ components, which are not effective in NMR:

$$\begin{aligned} B_x^+(t) &= -B\cos\left(\theta+\eta\right)\sin\sigma+B\sin\left(\theta+\eta\right)\cos\sigma \\ B_y^+(t) &= -B\cos\left(\theta+\eta\right)\cos\sigma-B\sin\left(\theta+\eta\right)\sin\sigma \end{aligned} \tag{4.12}$$

where $B=B_t(t)\,B_{co}\,s\left[\hat{a}_t\cdot\left(\cos\theta\,\hat{a}_x+\sin\theta\,\hat{a}_y\right)\right]/2$. These rotating frame components are enough to express magnetizations. For the sake of easiness, assume a small tip angle to obtain *x* and *y* components of the magnetization:

$$\begin{aligned} dM_x^+(t)/dt &\approx -\gamma\,M_o B_y^+(t) \\ dM_y^+(t)/dt &\approx \gamma\,M_o B_x^+(t) \end{aligned} \tag{4.13}$$

where γ is gyromagnetic ratio, M_o is the instantaneous magnetic moment per sample voxel immediately after applying a 90^o pulse. Note that, later in this chapter it will be shown that the

formulation is still valid for larger flip angles using a computer simulation [68]. Assuming a square pulse:

$$\begin{aligned} M_x^+(t) &= -\gamma\,\tau\,M_o B_y^+(t) \\ M_y^+(t) &= \gamma\,\tau\,M_o B_x^+(t) \end{aligned} \tag{4.14}$$

where τ is the duration of the pulse. Complex transverse magnetization of the ICRF coil magnetic field can be written as $M_{T,ICRF}^+(t) = M_x^+(t) + i\,M_y^+(t)$. Substituting Eq. (4.14) gives:

$$M_{T,ICRF}^+(t) = M_{T,ICRF}\,e^{i\theta}\left[\hat{a}_t \cdot \left(\cos\theta\,\hat{a}_x - \sin\theta\,\hat{a}_y\right)\right] \tag{4.15}$$

where $M_{T,ICRF} = \gamma\,\tau\,M_o\,e^{i\eta}\,e^{i\sigma}\,B_t(t)\,B_{co}\,s/2$. Remaining terms at the right side of Eq. (4.15) are directly related to the orientation of the ICRF coil. As the RF pulse scheme changes, the complex transverse magnetization of the ICRF coil changes similar to the anatomy case. However, the orientation related complex term in Eq. (4.15) makes a very important difference. In the first RF, unit vector of the transmit magnetic field will be $\hat{a}_t = \hat{a}_x$, because, its direction shows the *x*-axis. Substituting this information to Eq. (4.15) results with the first complex transverse magnetization of the ICRF coil as:

$$M_{0T,ICRF}^+(t) = M_{T,ICRF}\,e^{i\theta}\cos\theta \tag{4.16}$$

The second, third, and the forth transmit magnetic field unit vectors become $\hat{a}_y, -\hat{a}_x$, and $-\hat{a}_y$ respectively and one can generalize the p^{th} RF (or p^{th} TR) as:

$$M_{pT,ICRF}^+(t) = M_{T,ICRF}\left(e^{i2\theta}e^{ip\pi/2} + e^{-ip\pi/2}\right)/2 \tag{4.17}$$

Above equation states that the modified RF pulse scheme given in Figure 4.3 adds phase term $\left(e^{i2\theta}e^{ip\pi/2} + e^{-ip\pi/2}\right)/2$ to the ICRF signal.

For the particular case explained above, the signal expression can be given as:

$$S_{ICRF}(t) = \iint \left(M_{T,ICRF} \left(e^{i2\theta} e^{ip\pi/2} + e^{-ip\pi/2} \right) \right) e^{-i2\pi\left(k_x x + k_y y\right)} dx\, dy \Big/ 2 \tag{4.18}$$

Substituting Eq. (4.4) into Eq. (4.18) gives:

$$\begin{aligned} S_{ICRF}(t) = & \iint \left(M_{T,ICRF} e^{i2\theta}\, e^{-i2\pi k_y \left(y + N_y \Delta y/4\right)} \right) e^{-i2\pi k_x x} dx\, dy \Big/ 2 \\ & + \iint \left(M_{T,ICRF} e^{-i2\pi k_y \left(y - N_y \Delta y/4\right)} \right) e^{-i2\pi k_x x} dx\, dy \Big/ 2 \end{aligned} \tag{4.19}$$

This result can be interpreted graphically as well. Figure 4.4 shows the effect of the orientation of the ICRF coil. Assume, RF_1 is applied and the surface normal vector of the ICRF coil makes θ angle with RF_1. This excitation pulse can be decomposed into two orthogonal fields, $RF_{x'}$ and $RF_{y'}$, which are perpendicular and parallel components to surface normal vector of the ICRF coil, respectively. By using Faraday's law of induction, one can conclude that only the $RF_{y'}$ induces a current on the ICRF coil, and $RF_{x'}$ does not affect the coil. If one applies this operation to other components of the RF excitation pulses in Figure 4.3b, k-space constants become $m' = e^{i\theta}\left[\cos\theta,\ \sin\theta,\ -\cos\theta,\ -\sin\theta,\ \cos\theta \ldots\right]$ and $m'_p = m'_{p+4}$ (Figure 4.4).

In this case, not only the direction, but also the magnitude of the effective RF field changes in each TR. The disturbance in the k-space results with the change in the image space.

One can make mainly two important conclusions on this result and Eq. (4.19). First, the modified RF scheme causes shifting the original image. The anatomy shifts in phase encoding direction with an amount of $N_y/4$ pixels, on the other hand the original ICRF coil image shifts

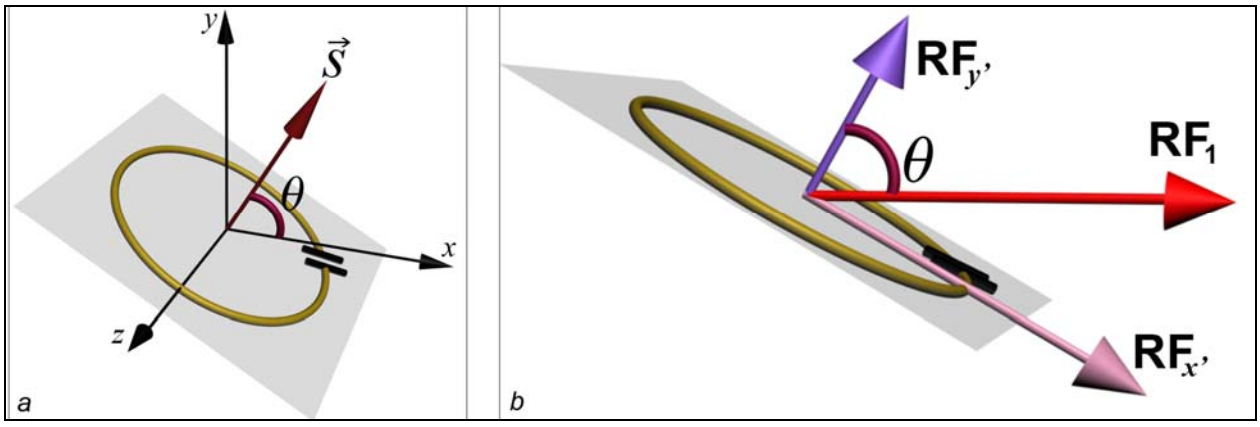

Figure 4.4: a) Interaction of the linear polarized RF and the ICRF coil. b) k-space lines result of circulating polarization vector.

in phase direction and the ghost shifts in reverse direction. As a result, one copy of the ICRF coil stays in the shifted the anatomy image and the other copy shifts $N_y/4$ pixels in the opposite direction, which can be color-coded and inserted into the anatomy image. Although the exact location of the original image is not known, the center line of the shift y_o, from where the image needs to be cut and paste to the anatomy image, is related to the total number of phase lines and number of pulses in one turn and given by $y_o = N_y - 2N_y/P$, where $P = 4$ in above example. As a result, for the particular case, $P = 4$, $y_o = N_y/2$ which is equal to the center of the image.

Secondly and more importantly, the phase difference of the ICRF coil and ghost images is two times of the orientation of the ICRF coil, 2θ. In order to find the phase difference between the shifted ICRF coil images, weighted average [69] needs to be calculated. For $P = 4$ case, the center of the image is the border of the shifted images. Cutting one side and multiplying with the conjugate of the other side of the image provides weighting. Phase of the mean value gives the weighted average's phase, 2θ which is two times of the absolute orientation of the ICRF coil.

$P = 4$ case is the easiest and convenient one, but a more general formula for an arbitrary *P,* the anatomy and the ICRF coil signals can be expressed as:

$$
\begin{aligned}
S_{Anatomy}(t) &= \iint \left(M_{T,Anatomy}\, e^{-i2\pi k_y \left(y - N_y \Delta y/P\right)} \right) e^{-i2\pi k_x x}\, dx\, dy \\
S_{ICRF}(t) &= \iint \left(M_{T,ICRF} e^{-i2\pi k_y \left(y - N_y \Delta y/P\right)} \right) e^{-i2\pi k_x x}\, dx\, dy \Big/ 2 \\
&\quad + \iint \left(M_{T,ICRF} e^{i2\theta}\, e^{-i2\pi k_y \left(y + N_y \Delta y/P\right)} \right) e^{-i2\pi k_x x}\, dx\, dy \Big/ 2
\end{aligned}
\tag{4.20}
$$

where the shift is N_y/P pixels. Eq. (4.19) shows when number of RF pulses in one turn is four and shifting is $N_y/4$ in one direction. Shifting mechanism can be changed by changing the number of turns P, that is, the amount of shifting can be increased by decreasing the value of P and vice versa. Above formulae are derived using small flip angle approximation, which means no transverse component of the magnetization is left at the end of the TR, in order to obtain a simple and general equations.

Although the small flip angle is an important assumption, generalization of the method can be done. For this, implementation of the method to a more general real-time sequence with a high flip angle will also be shown. TrueFISP, which is a very common fast imaging sequence, works with high flip angles. A MATLAB simulation code for TrueFISP sequence can be used to show the shifting mechanism is still valid for larger flip angles. TrueFISP sequence is highly dependent on field inhomogeneities. In order to understand signal behaviors of the anatomy and the ICRF coil computer simulations were conducted using MATLAB. Anatomy and catheter signals were obtained using following parameters: T1 200 ms, T2 60 ms, TR 5.8 ms, TE 2.9 ms, flip angle 50^0. Figure 4.5 shows the simulation where the ICRF coil, ghost, and anatomy can be seen. As a result, one can conclude that the formulation is still valid for higher flip angles. Furthermore, TrueFISP sequence is based on gradient echo imaging principles but steady state signal varies drastically. Simulation results also show that the anatomy, ICRF coil, and ghost signals differ significantly as a function of field inhomogeneity.

As shown in Figure 4.5, in addition to the anatomy and the ICRF coil signal, ghost of the ICRF coil is observed similar to small tip angle approximation case. The same figure shows that the ICRF coil and its ghost have the same shape against the field homogeneity, but there is 180^o phase difference. This property adds one more parameter for the method, because; signal amplitudes of the ICRF coil and its ghost can be changed by adjusting field inhomogeneity. The validity of the formulation with high flip angles will also be supported by the results

4.3. Method

In the present study, the aim is to separate the anatomy and the interventional devices using a linearly polarized birdcage body coil. The identical RF pulse shape with changing amplitude and direction is used to excite feed the body birdcage coil.

The quadrature hybrid is eliminated and the birdcage body coil is used as a two channel linear transmit-only coil to create one copy of original the anatomy image and two copies of the ICRF coil image to reconstruct a color-coded image. FLASH and TrueFISP sequences are modified and turning linearly polarized field is obtained by using the transmit array system.

In our work we used a 3 tesla Siemens TIMTrio and an 8-channel transmit array systems. Siemens body and spine matrix coils are used for reception. In the phantom experiments,

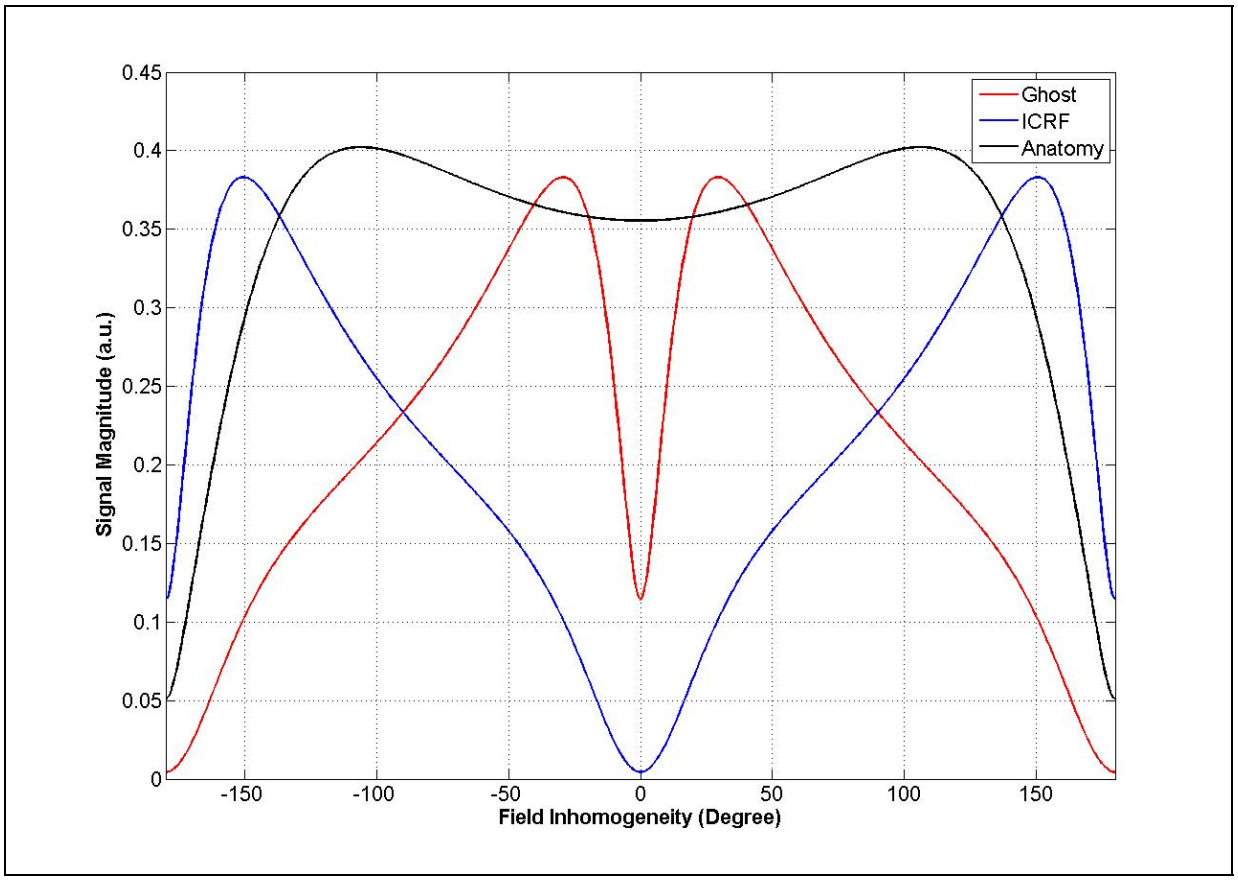

Figure 4.5: Simulation result for TrueFISP.

.images acquired using spine array phased array coils in both transmit and receive array experiments. A MATLAB code is written for the reconstructions as well as the color coding

.

4.3.1. Rotational Orientation:

Two different ICRF coils with different diameters, and the same length, were constructed for the rotational orientation experiments. The first ICRF was 100-mm long and constructed on a 6 F Teflon catheter using coated copper wire 0.4 mm in diameter; a heat shrink tube was used for isolation resulting in a prototype device with an outer diameter of 3 mm (9 F). It was tuned by a 22 pF ceramic chip capacitor to 123.23 MHz using an HP 8753D network analyzer. The second ICRF coil had the same length with 22 F total diameter. A rectangular 15 cm × 10 cm × 30 cm oil phantom was used (Figure 4.6a).

In order to control the amount of rotation, a Smith chart was used (Figure 4.6a). Before each acquisition, the ICRF coils rotated equally. A simulation was done for changing rotational orientation of the ICRF coil for proof of principle.

4.3.2. Catheter Tracking

The first ICRF coil, 9 F, was also used in imaging experiments. The ICRF coil is used similar to our previous study [25]. The same oil phantom was used and three straws filled with potassium chloride (KCl) solution were inserted into the phantom.

4.3.2.1. Flash

Flash sequence is modified in order to get circulating polarizations with following parameters: TR 9.8 ms, TE 4.1 ms, slice thickness 5 mm, flip angle 30^o, FOV 300X300, imaging matrix 256X256,

4.3.2.2. TrueFISP

TrueFISP sequence is highly dependent on field inhomogeneities. In order to understand signal behaviors of the anatomy and the ICRF coil computer simulations were conducted using MATLAB. The anatomy and catheter signals were obtained using following parameters: T1 200 ms, T2 60 ms, TR 5.8 ms, TE 2.9 ms, flip angle 50^o.

In addition, proof of principle experiments were conducted with a modified TrueFISP sequence using following parameters was used: TR 5.8 ms, TE 2.9 ms, slice thickness 5 mm, flip angle 50^o, imaging matrix 256X256.

4.3.3. Transmit Array Calibration

Two channel of the transmit array system have been used. After each boot of the system, the phase difference between the channels changes. Therefore, before each experiment, the phase difference is calibrated using the reverse polarized mode. Spins are forward polarized, if the body birdcage coil is adjusted to produce the reverse polarization mode, no signal is received.

The reverse polarization mode is obtained by two RF pulses with the same amplitude and the 90^o phase difference. Before the experiment, phase of the y-channel is scanned between 40^o to 140^o with 10^o increment. The image with a minimum signal level is assumed to be the reverse

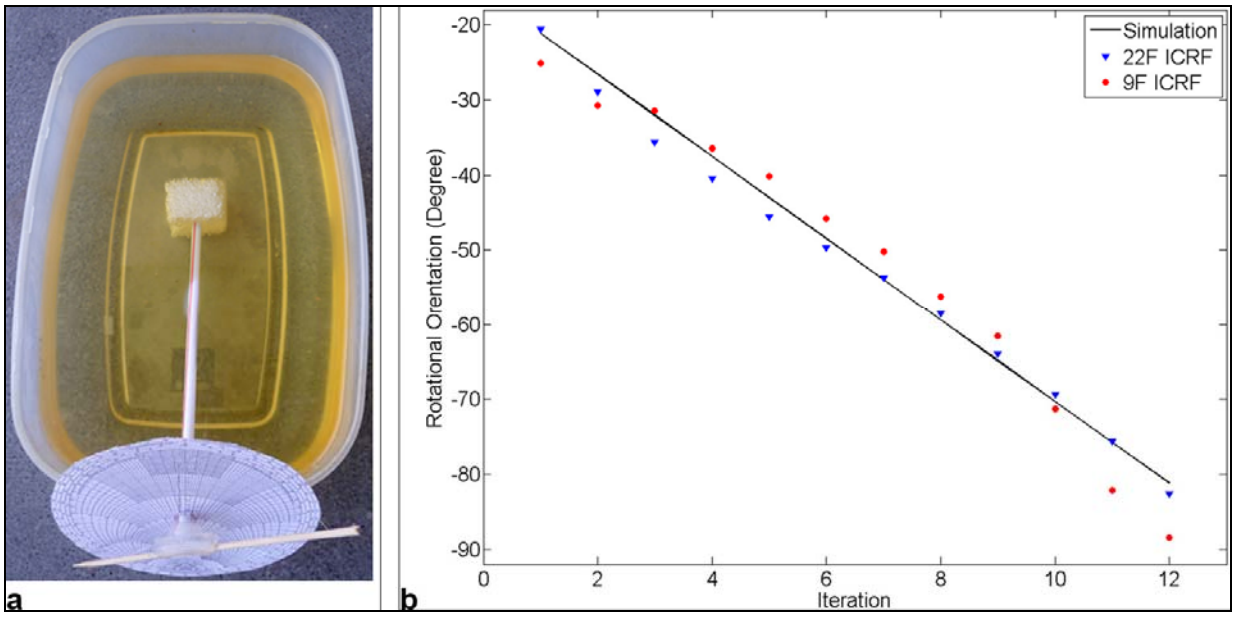

Figure 4.6: a) Phantom setup. The same phantom was used for imaging experiments. b) Result of the rotational orientation experiment.

polarized mode of the image. After fine tuning, the relative phase between the *x*- and *y*-channels is found.

4.4. Results

4.4.1. Rotational Orientation of the ICRF Coil

Figure 4.6 shows rotational orientation experiment setup and the results obtained using two different ICRF coils. In each iteration, the ICRF coils rotated one unit, which is approximately equal to 5o. Experiment showed very high correlation with the simulation result.

4.4.2. Tracking of the ICRF coil

4.4.2.1 Flash

Figure 4.7a shows a reference transversal image in order to show the original data without using oscillated RF field. In the result of the steering RF catheter tracking method, the anatomy was shifted up, on the other hand, ICRF coil was shifted both up and down. Different *P* values causes different amount of pixel shifting. Figure 4.7b and c show *P* equals 16 and 8 respectively. There are two other important parameters to change characteristics of the shifting. One of them is turning direction of the polarization vector. Figure 4.8a shows color-coded image of counter-clockwise turn of the vector with $N = 4$.

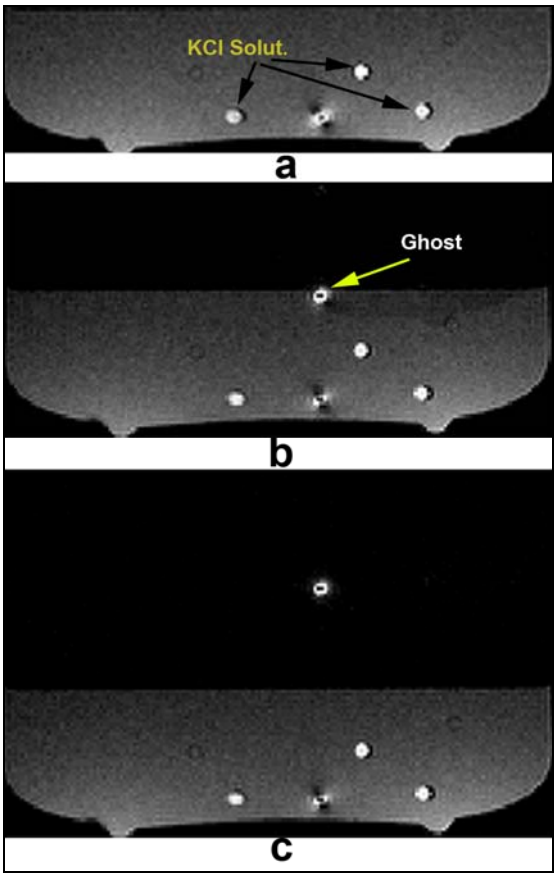

Figure 4.7: Transversal images of the method with varying number of turns, *N*. Images show that the amount of shifting pixel can be adjusted. a) Original image $P = 1$. b) $P = 16$. c) $P = 8$.

Shifting the turn direction to clock wise direction swaps the anatomy image and the ghost (Figure 4.8b). Furthermore, phase encoding direction is anterior-posterior (A-P) in Figures 4.8a and b. Modifying the phase encoding direction to left-right (L-R) changes the whole image (Figure 4.8c). As a result, there are three significant parameters to be manipulated according to application or imaging plane: *P*, vector turn, and phase encoding directions.

Lastly, Figure 4.10 shows the result of different parameters and imaging planes using TrueFISP sequence. Figure 4.10a, b, and c are transversal, Figure 4.10d is an oblique image, and Figure 4.10e is a coronal image. Oil signal is high and signal of water in straws are weak in Figure 4.10a because of the resonance frequency. On the other hand, water signal is very high in Figures 4.10 a and b. At the same time signals of the ICRF coil and its ghost change. Figures 4.10 d and e shows oblique and coronal images respectively, but shimming on those planes are not as easy as transversal case, therefore phantom image is not homogeneous.

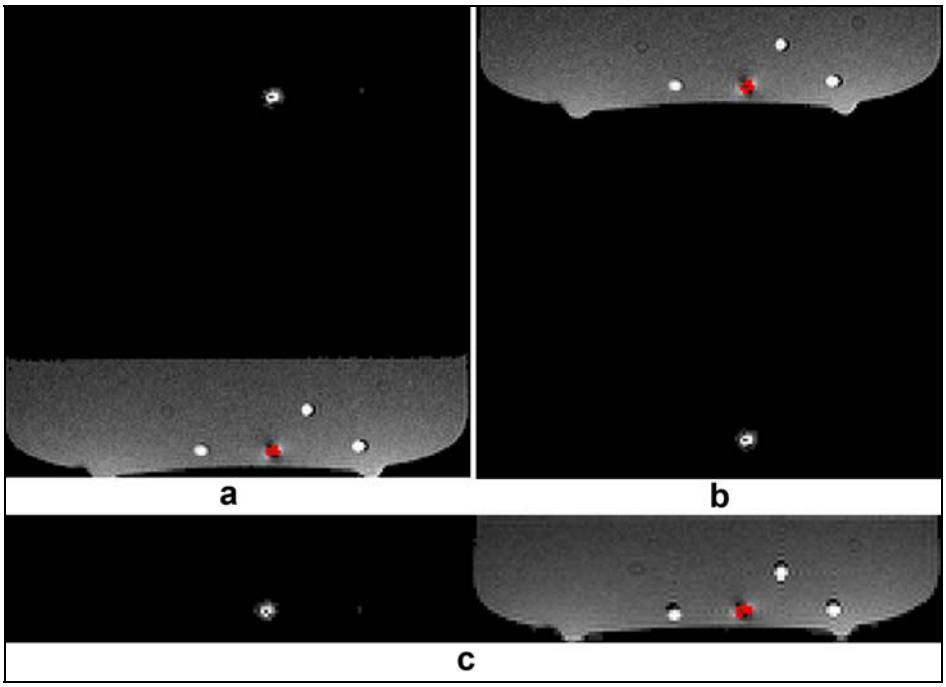

Figure 4.8: Color-coded images with changing parameters. a) Polarization vector turns counter-clockwise direction and phase encoding direction is A-P. b) Polarization vector turns clockwise direction, same phase encoding direction with a. c) Polarization vector turns counter-clockwise direction and phase encoding direction is L-R.
The method works with different imaging planes: Coronal (Figure 4.9a), sagittal (Figure 4.9b), and oblique (Figure 4.9c).

4.5. Discussion

A similar modulation of the phase and the magnitude occurs when a wire is used instead of an ICRF coil, because, the current induced on the wire is also dependent on the phase of the excitation field [70]. As the phase of the excitation changes, the phase of the current on the wire changes and as a result, field profile at the vicinity of the wire changes. This disturbance affects the k-space lines and a similar shifting occurs as the ICRF coil case.

Here, the principle behind the detection of the ICRF coil is the orientation dependence of the induced current and the field created by this current. In the anatomy image case, there is only the phase modulation and this causes the shift of the anatomy image. On the other hand, as the phase of the RF excitation field changes, the characteristics of the field created by the induced current on the ICRF coil varies. As a result, in the vicinity of the ICRF coil not only the phase but also the magnitude is modulated. Furthermore, both phase and magnitude modulation mechanisms occur different than the anatomy case. The modulations in the k-space can be calculated analytically or by a computer simulation.

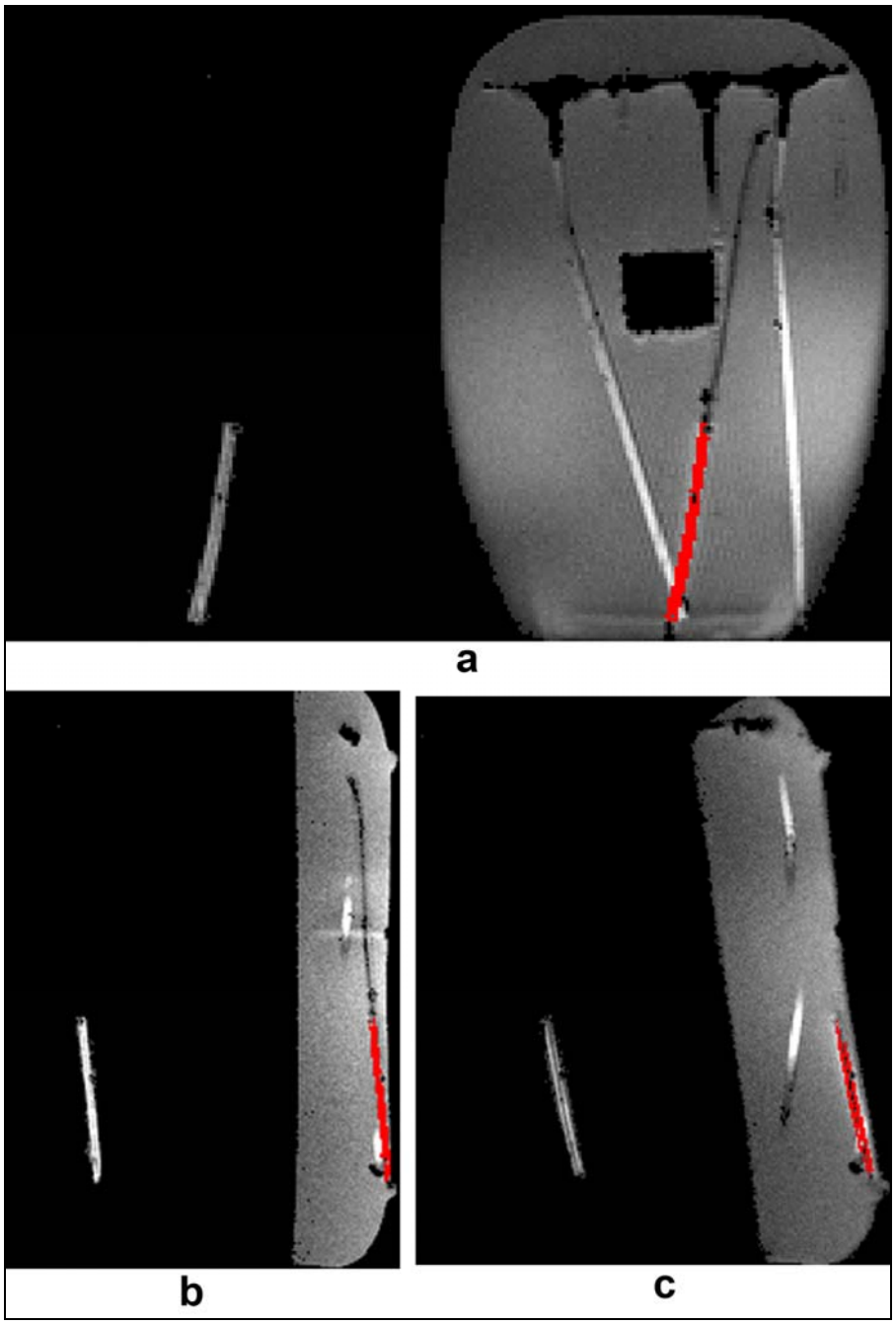

Figure 4.9: Color-coded images of different planes. a) Coronal image. b) Sagittal image. c) Oblique image.

In our site, the *x*-channel of the body coil was performing significantly worse than the *y*-channel. Therefore oil is used in the phantom experiments, because it helps to avoid dielectric effect-related inhomogeneities [62]. In addition, the same signal level from the individual body coil channels is obtained only when the *y*-channel is multiplied by 0.67, while the multiplier of the *x*-channel is kept at 1.00 using the transmit array system. Therefore, oil phantom is used to obtain the homogeneous reverse polarization mode of the image which is difficult.

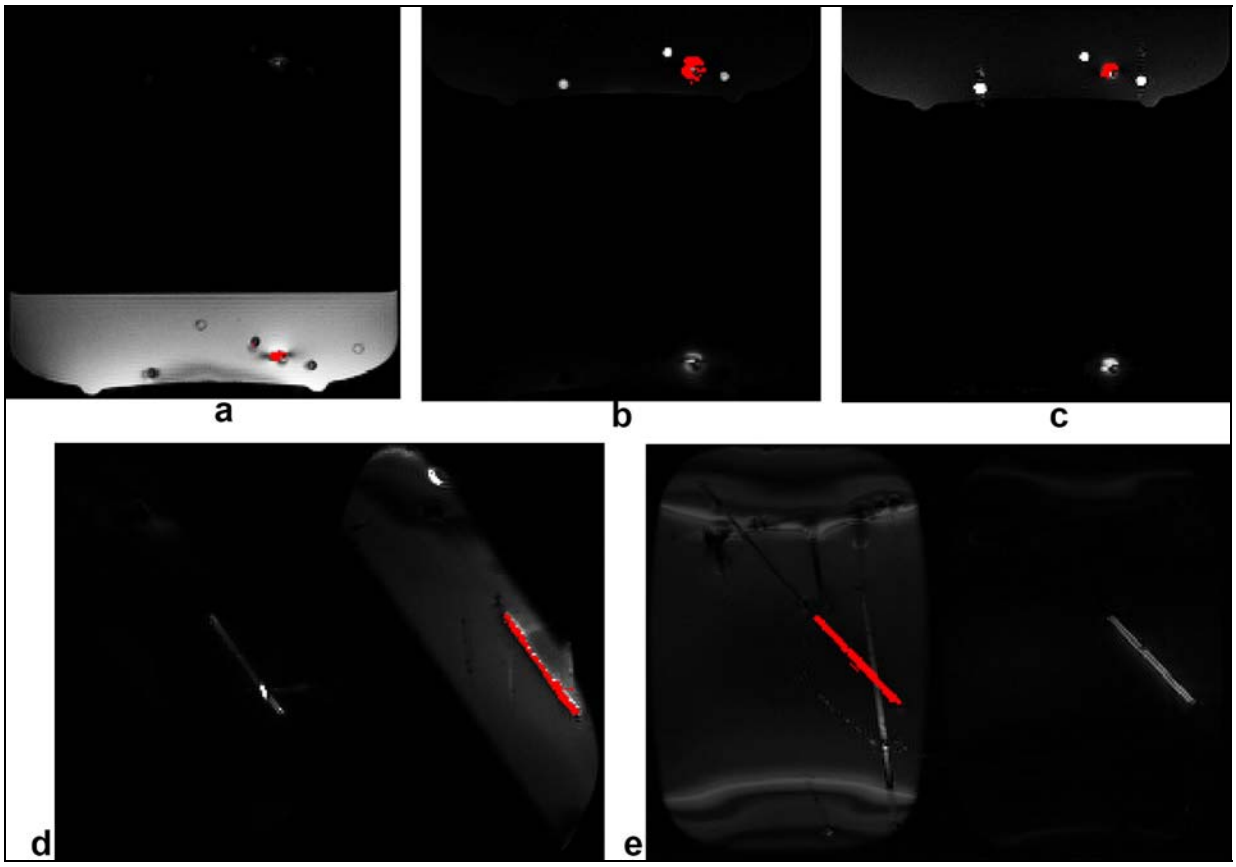

Figure 4.10: Imaging experiment results of TrueFISP sequence. a, b, and c shows transversal images with different oil and KCl solutions. a) High oil signal intensity. b) High KCl solution intensity with suppressed oil signal. c) Highest KCl solution signal intensity with residual oil signal. d) Oblique plane with low oil signal intensity. e) Coronal plane with low background signal intensity.

Siemens transmit array system can operate 8 channels with different phases and amplitudes. Furthermore, each channel can be fed with different pulse shapes. In our applications, we use only two channels and manipulate phases and amplitudes. Therefore, we do not utilize the system completely, but using the body coil is much more convenient for accessibility and liability. It is already embedded the imager and because of using only two channels, it is simpler deal with.

As stated above, a forward polarized excitation has a better SAR performs than a linear excitation. The linear polarization (Figure 4.2) doubles average SAR and quadruples peak SAR. On the other hand, this is not valid with modified circulating linear RF excitation. Its average body SAR is still two times more than forward excitation, but peak SAR is also two times more, because the electric field vector changes at a point of interest from TR to TR. For $P = 4$, the electric field at a point drops such that SAR becomes two times of the forward polarization case. As a result, peak and average SAR of the modified circulating RF excitation

is doubled as compared to conventional excitation. The conventional SAR calculation can be used and halving the limit keeps the new design in safety limits.

4.6. Conclusion

This study presented a novel method to simultaneously acquire the rotational orientation of the ICRF coil and track the coil built on a catheter. First, the anatomy and the ICRF coil images are separated, then orientation is calculated and color-coded image of the ICRF coil is reconstructed for tracking. Phantom experiments have been demonstrated the proof-of-principle of the method using both FLASH and TrueFISP sequences.

5. Inductively Coupled Birdcage Coil

5.1. Introduction

In previous chapters in this dissertation, the birdcage coils have been mentioned as volume coils, such as body and receive-only coils. Standard birdcage [35] coil is used widely since it is first introduced in 1985 by Hayes *et. al.* There are two main advantages of the birdcage coil: first, it creates homogenous magnetic field; second; it can be built as quadrature coil easily. Standard quadrature birdcage coils are design to be sensitive to circularly polarized magnetic field. This is done by the help of a quadrature hybrid circuit (Figure 2.1). Although birdcage coils are essential elements of modern MRI scanners, they have never been used as ICRF coils. ICRF coils [22] are simple wire loops resonated using a capacitor. They have been used for small FOV imaging [23, 24] and also catheter tracking [21, 25]. They are used to amplify transmit and receive signals in close vicinity. When a pair of back-to-back diodes is connected parallel to the resonating capacitor, coupling to transmit field is eliminated and only receive coupling remains. These coils are called receive coupled radiofrequency (RCRF) coils [25, 71]. RCRF coils are safer as compared to ICRF coils [25].

The reverse polarization is our main focus and it is used effectively in different applications and methods. The ICRF coil is a linearly polarized signal generator which contains a reverse polarized field component. However, it is impossible to eliminate the forward component of the ICRF coil. So, a design for the reverse polarized signal source was investigated. Because we are very familiar with the birdcage coil design, we decided to make simulations. As a result, it was observed that the conventional mode of a birdcage coil generates a reverse polarized field outside of the birdcage coil. On the other hand, inductive design was built to examine if it could work without feeds and it became successful. The ICRF have never been miniaturized for placement inside body orifices. In this study, birdcage coil is miniaturized and used as an inductively coupled RF coil.

The new design can be used as an internal coil for prostate biopsy. Furthermore, it can be constructed on a catheter for tracking the interventional devices and imaging vessel walls. Lastly, it can be used for intestine and esophagus imaging.

5.2. Theory

As opposed to conventional birdcage coils, the new design is used inductively, thus there is no feed point for transmission, reception, or decoupling. In addition, it is symmetric with respect to all axes. They are small and do not affect the tuning and noise profile of the external coil. If one reverses a conventional volume birdcage coil in z-axis, the signal inside the coil becomes reverse polarized. However, coupled birdcage designs are immune to orientation, i.e. it can work in all orientations.

Since ICBC coils have two intrinsic orthogonal modes of operation (*x* and *y* directed), the transverse component of the magnetic field sensitivity exists in all orientations. For example, if the axis of the ICBC coil is directed to the x-axis (as opposed to the z-axis in its optimum use), one of the modes will be in the y-axis. Therefore the coil's sensitivity will remain. In one mode of the operation, the transmit magnetic field induces current on the ICBC coils. This induced current amplifies the flip angle around it. When an external coil such as a birdcage coil is used in reverse polarization mode [25] as a receiver, the external coil does not pick-up any signal from the anatomy directly, but only from the anatomy in the vicinity of the ICBC coil. Similarly, when an external birdcage coil is driven in reversed polarized mode, the magnetization in the anatomy will not be flipped in any location but only around the vicinity of the ICBC coil.

These coils can be used without modifying the scanner hardware and do not affect tuning of external coils. ICBC coils are not connected to the scanner by wires; rather the MR signal picked up by these coils is transferred to a receiving coil by induction. Therefore, this design is system independent.

The signal inside and outside the inductive designs depend solely upon the mode of the external transmit and receive coils. Coupled birdcage coils produce forward polarized field inside the coil. On the other hand, the outside of the coil is the source of the reverse polarized signal. If an external birdcage coil or a phased array coil is used for reception, forward (or reverse) polarization mode of this coil makes the inductive birdcage coil work in forward (or reverse) mode (Figure 5.1).

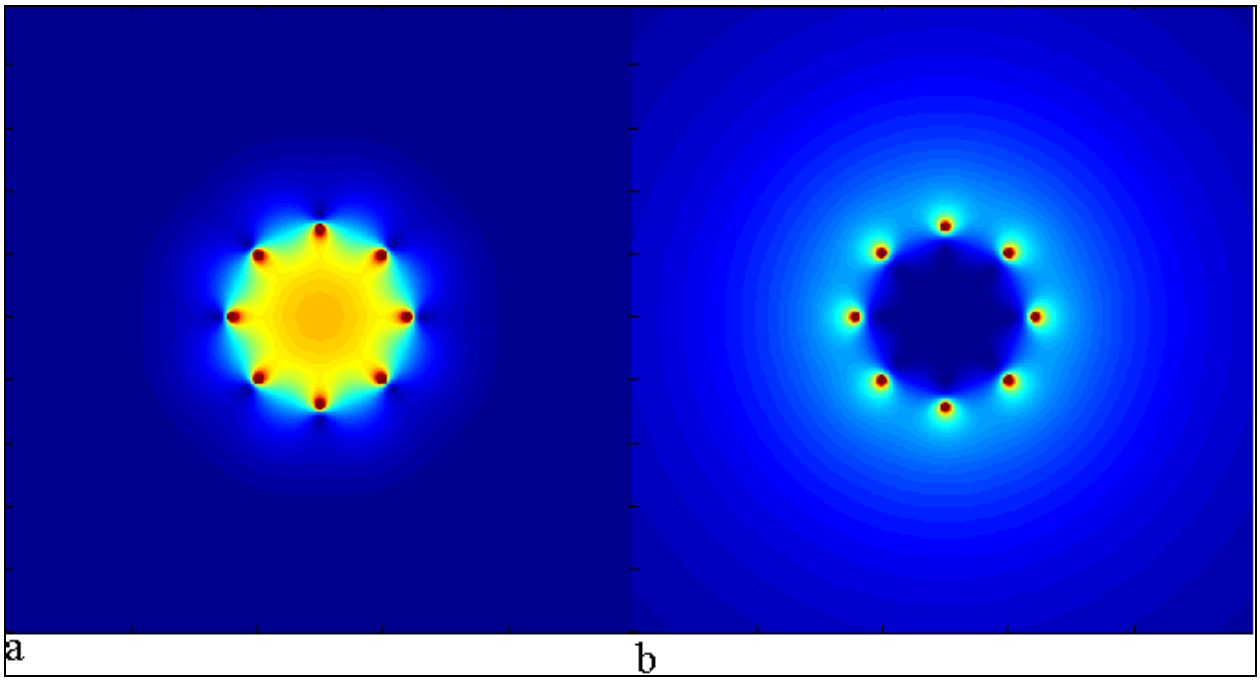

Figure 5.1: Simulation of eight legs highpass inductively coupled birdcage coils. a) Forward mode of ICBC b) Reverse mode of ICBC.

5.2.1. External Coils

CBC coils work by coupling to external coils. Characteristics of CBC coils vary according to transmit and receive polarizations of the external coils. Any combination of these transmit and receive coils will result in different field distribution and SNR inside and around the CBC coils. For example, in order to visualize around the ICBC coil and suppress remaining part of the anatomy, reverse transmit and reverse receive external coil couple should be used.

Transmit or receive coil types can be branched by their polarizations. Forward polarized birdcage coil transmit mode is used by conventional birdcage coils (such as body, extremity, and head coils). Inductive (ICRF and ICBC) coils are coupled, but receptively coupled (RCRF and RCBC) coils are weakly coupled to forward birdcage transmit mode due to back-to-back diodes. Note that if excited, ICRF and RCRF coils produce a linear field and ICBC and RCBC coils produce a forward polarized field inside, and reverse polarized field outside of themselves.

On the other hand reversing the birdcage coil or switching the cables enables the reverse polarized field. Spins cannot be excited, receptively coupled coils (RCRF and RCBC coils) are

weakly excited, and inductive coupled RF coils (ICRF and ICBC coils) are excited by using a reverse polarized transmit field.

Linearly or elliptically polarized coils behave similar to forward polarized coils. Spins and inductive (ICRF and ICBC) coils are coupled, receptively coupled (RCRF and RCBC) coils are weakly coupled to linear coils. On the other hand, linear, elliptic, forward, and reverse polarized transmissions can be constructed by a phased array coil using proper weightings.

As opposed to transmit modes of the external coils, the receive coils vary slightly. Most significant case is the reverse polarized mode of receive coils. In this case, the ICRF, RCRF and the outside of ICBC and RCBC coils are coupled to the reception of reverse polarized birdcage coils. Spins are completely decoupled from this mode, so this mode is useful for suppressing the anatomy. On the other hand, forward polarized birdcage coil reception mode belongs to conventional birdcage coils. It is coupled to forward and linear polarized modes, that is, spins, ICRF, RCRF, and the inside of ICBC and RCBC coils. In all other receive coils, phased array, linearly and elliptically polarized coils, all possible signal sources can be coupled, but proper weightings can make it possible for phased array coils to receive linear, forward and reverse polarized signals. In order to utilize ICBC and RCBC coils, any combination of transmit and receive modes mentioned above can be used according to applications. A coil can be made transmit only, receive only, and transmit-receive. Different polarizations are possible by either hardware, or software [25, 72].

5.2.2. Modes of Birdcage Coil

Modes of inductively coupled birdcage coils are similar to active case [53]. The circuit of the birdcage coil is represented by the ladder network, and the current on each loop is represented by sinusoidal equations. The number of solutions (or modes) is related to number of legs. The first mode, $m = 1$, is the most homogenous solution.

5.3. Method

Two different highpass birdcage coils were built to examine different modes of the ICBC coils. 136 pF (ATC, USA) ceramic chip capacitors were used to resonate $m = 1$ mode in one of the high pass birdcage coils. On the other hand, a 110 pF capacitor was used to resonate $m = 2$ mode. Small birdcage coils were tuned using an HP 8753D network analyzer and examined

with Siemens TIMTrio 3 T imager. The coils have 38 mm inner and 40 mm outer diameters tuned to 123.23 MHz. The legs are 100 mm long and 2.5 mm wide (Figures 5.2 and 5.3). They are placed on the outer surface of the acrylic cylinder. The insides of the coils were filled with saline solution in order to show the inside characteristics of coils.

Phantom imaging experiments were conducted to study the reverse polarization technique in ideal conditions. In these experiments, the ICRF coils were inserted into a gel filled bottle. Axial and sagittal images were acquired using a gradient echo sequence with 40^{o} flip angle. The following gradient echo parameters were used: TR/TE: 40/3.4 ms; spacing: 1 mm; slice thickness: 5 mm; matrix: 256 X 256; FOV: 300 X 300 mm^2. Quadrature body coil was used as the external coil. All transmit/receive combinations of the external coil were examined; a) forward transmit and receive, b) forward transmit, reverse receive, c) reverse transmit and receive, d) reverse transmit and forward receive.

5.3.3. Tuning Coupled Birdcage Coils:

In order to tune a coupled birdcage coil, a multi turn search coil was connected to a network analyzer. Then, it was inserted into the coil of interest. The four legs highpass birdcage coil has three modes. The first and the second modes can be observed by an analyzer when the search coil is rotated on its longitudinal axis (Figure 5.4). In order to tune one of the modes, during rotation, the resonance frequency should not have been changed. On the other hand, endring mode was visible as the search coil was brought closer to endring.

Figure 5.2: A picture of the high-pass inductively coupled birdcage coil used in experiments.

Figure 5.3: A picture of the high-pass ICBC coil. Capacitors can be placed inside, outside, and on the endrings. Here, the capacitors are placed inside of the coil.

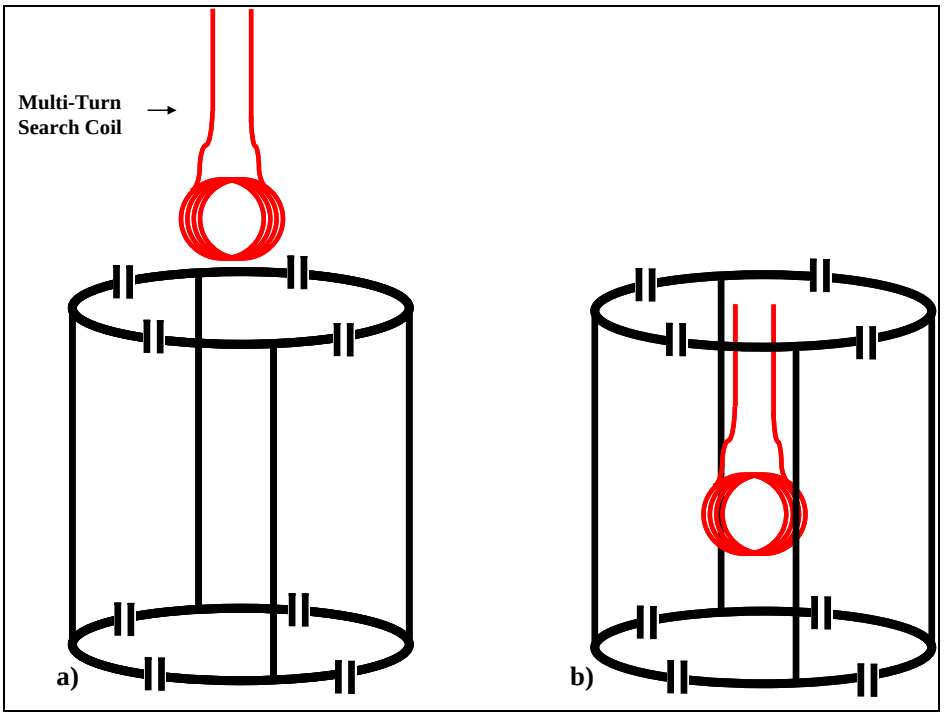

Figure 5.4: Tuning method of the coupled birdcage coils.

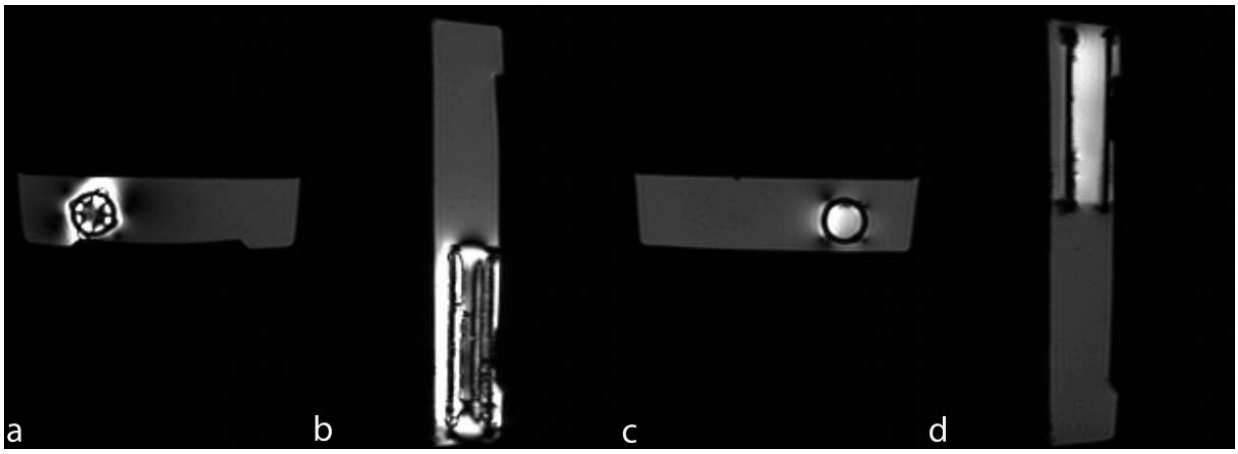

Figure 5.5: Forward transmit and forward receive mode. Window/Level are the same for all images. a) Axial image of mode 1 b) Sagittal image of mode 1 c) Axial image of mode 2 d) Sagittal image of mode 2.

5.4. Results

Normally, mode 1 of the birdcage coil is relatively homogenous in comparison to mode 2, but the high flip angle amplification in Figures 5.5 a and b disturbs homogeneity. On the other hand, this amplification shows possible SNR improvement.

Two aspects are important in Figure 5.6. Firstly, the anatomy signal suppression and secondly, the intensity of the flip angle amplification.

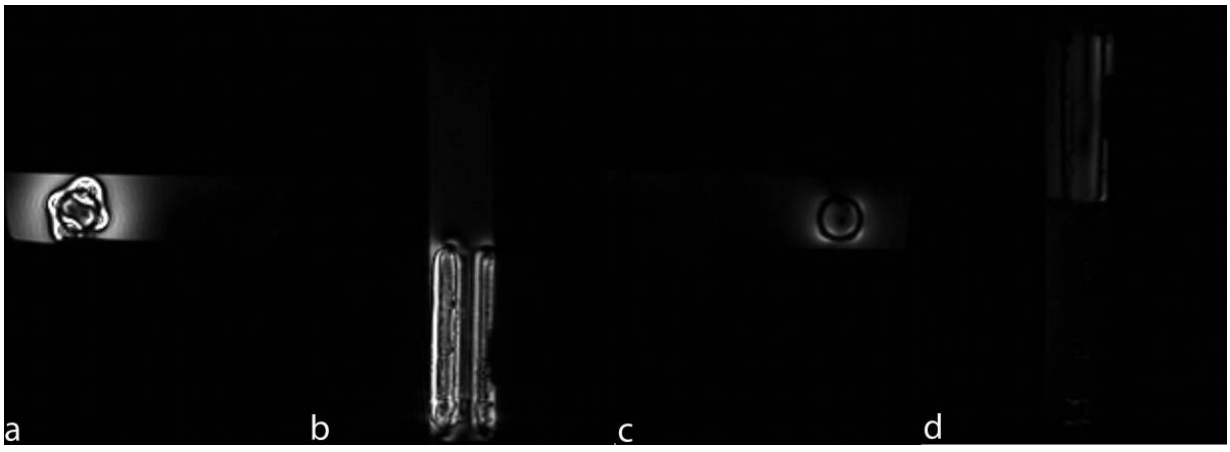

Figure 5.6: Reverse transmit and reverse receive mode. Window/Level are the same for all images. a) Axial image of mode 1 b) Sagittal image of mode 1 c) Axial image of mode 2 d) Sagittal image of mode 2.

5.5. Discussion

The powerful properties of the inductively coupled birdcage coils explained in this study make them very attractive as internal and catheter coils. Among many possible applications, this design is very suitable for the imaging of the prostate when it is placed inside the rectum.

For an external coil, homogeneity is very important issue. On the other hand, we can ignore homogeneity and use different modes of inductively coupled design. For example, endring mode can be used for forward imaging. In addition, building and expanding inductively coupled birdcage coil would provide both m=1 and endring modes.

The new method suppresses anatomical information to improve imaging of the prostate, vagina, uterus, vessels and different walls such as the colon, esophagus, and trachea. Small pill sized coils can be used to image the small intestine under MRI. In addition to imaging, the reverse polarization component of the ICBC coil can be used for spectroscopy as well.

One other application can be catheter tracking. Constructing an ICBC coil on the interventional devices would help provide very effective catheter tracking. Switching between the forward and reverse mode of the coils would result with a flickering catheter, which provides good visualization of the device. The ICBC coil can be used to calibrate MR imaging coils. If a perfect quadrature and ICBC coils are used, the ICBC coil produces a signal only inside in forward mode, and outside in reverse mode.

Using this property may help to test a quadrature coil. Furthermore, the reverse polarization mode of a phased array coil requires a more complex procedure than the reverse mode of a quadrature coil. Linearity of coil elements, sensitivity maps, and calibration of the coil affect the implementation. Similar to the previous item, the ICBC coil can be used to increase the effectiveness of the reverse polarization method for phased array coils. Lastly, ICBC coils can be used to increase fiducial marker visibility.

To conclude, a new birdcage design as internal coil is proposed. Effectiveness of the new design was shown by phantom images comparing with an active loop coil. Using transmit array system enabled forward and reverse transmissions.

6. CONCLUDING REMARKS

Although X-ray provides precise and fast localization of the interventional devices, ionizing radiation and poor soft tissue contrast are drawbacks of the modality that need to be considered. On the other hand, interventional MRI is a promising minimally invasive alternative to risky surgical procedures. MRI is a non-ionizing modality with high soft tissue contrast. However, as opposed to X-ray, interventional devices are not visible under MRI. Various techniques have been developed for identification of interventional devices.

The studies in this dissertation are based on the reverse polarization method. The reverse polarization had been useless until the introduction of the reverse polarization method, because it is a mode of magnetic field that is not sensitive to anatomy signal. On the other hand, the ICRF coil, which generates both forward and reverse polarized field, can be used to utilize the reverse polarization mode. In this dissertation, improvement in tracking and visualization of the ICRF coil constructed interventional devices is presented using the reverse polarization.

Our first study enabled a very new technique for catheter tracking and also the idea paved the way of different applications. The feasibility of background suppression using a reverse polarization mode signal in catheter tracking using inductively coupled RF coils was demonstrated. With a single birdcage coil, both reverse and forward polarization mode signals were obtained. Imaging of the target object with a real-time imaging sequence using the forward polarization mode signal was possible and the catheter was distinctly seen in the reverse polarization mode signal. Color-coding enabled simultaneous visualization of catheter and anatomy without any restriction on the pulse sequence. The effectiveness of this method was tested by phantom and animal experiments.

The second study was an extension of the first one, but was a big step through the usability of the reverse polarization method. In this study, the feasibility of the reverse polarization method was examined using the transmit and receive array systems in two different applications of the method, i.e. catheter tracking and fiducial marker visualization. Using both transmit and receive RF coil arrays coupled to RCRF and ICRF coils, we showed that the method achieved successful background suppression in both phantom and volunteer studies.

The third technology we presented in this dissertation comprises a very exciting property for magnetic resonance imaging. Rotational orientation information for X-ray angiography is a straight forward detail. However, it is a very hard challenge for MRI. This new method not only provides positional but also offers rotational orientation information. This study presented a novel method to simultaneously acquire the rotational orientation of the ICRF coil and track the coil built on a catheter. First, the anatomy and the ICRF coil images are separated, then orientation is calculated and color-coded image of the ICRF coil is reconstructed for tracking. Phantom experiments have been demonstrated the proof-of-principle of the method using both FLASH and TrueFISP sequences.

Lastly, inductively coupled birdcage coil enabled a standalone imaging possibility with independence from scanner manufactures. In this study, a new birdcage coil design without any matching and active decoupling circuits, amplifiers, and wire connectors is introduced. Similar to inductively coupled RF coils, the standalone birdcage coil design couples to the external receive coil inductively. The main advantage of the standalone design is being independent from scanner manufactures.

We believe that studies in this dissertation are contributions toward obtaining better imaging systems, thus intervention lists will be able to conduct very difficult procedures successfully and many lives will be saved. The future study subjects of the author will be clinical studies in order to show the feasibilities of the methods.

7. BIBLIOGRAPHY

[1] J. H. Seppenwoolde, M. A. Viergever, and C. J. Bakker, "Passive tracking exploiting local signal conservation: the white marker phenomenon," *Magn Reson Med,* vol. 50, pp. 784-90, Oct 2003.

[2] M. Stuber, W. D. Gilson, M. Schar, D. A. Kedziorek, L. V. Hofmann, S. Shah, E. J. Vonken, J. W. Bulte, and D. L. Kraitchman, "Positive contrast visualization of iron oxide-labeled stem cells using inversion-recovery with ON-resonant water suppression (IRON)," *Magn Reson Med,* vol. 58, pp. 1072-7, Nov 2007.

[3] R. Dharmakumar, I. Koktzoglou, R. Tang, K. R. Harris, N. Beohar, and D. Li, "Off-resonance positive contrast imaging of a passive endomyocardial catheter in swine," *Phys Med Biol,* vol. 53, pp. N249-57, Jul 7 2008.

[4] R. R. Edelman, P. Storey, E. Dunkle, W. Li, A. Carrillo, A. Vu, and T. J. Carroll, "Gadolinium-enhanced off-resonance contrast angiography," *Magn Reson Med,* vol. 57, pp. 475-84, Mar 2007.

[5] O. Unal, J. Li, W. Cheng, H. Yu, and C. M. Strother, "MR-visible coatings for endovascular device visualization," *J Magn Reson Imaging,* vol. 23, pp. 763-9, May 2006.

[6] J. J. Krueger, P. Ewert, S. Yilmaz, D. Gelernter, B. Peters, K. Pietzner, A. Bornstedt, B. Schnackenburg, H. Abdul-Khaliq, E. Fleck, E. Nagel, F. Berger, and T. Kuehne, "Magnetic resonance imaging-guided balloon angioplasty of coarctation of the aorta: a pilot study," *Circulation,* vol. 113, pp. 1093-100, Feb 28 2006.

[7] M. E. Miquel, S. Hegde, V. Muthurangu, B. J. Corcoran, S. F. Keevil, D. L. Hill, and R. S. Razavi, "Visualization and tracking of an inflatable balloon catheter using SSFP in a flow phantom and in the heart and great vessels of patients," *Magn Reson Med,* vol. 51, pp. 988-95, May 2004.

[8] P. Magnusson, E. Johansson, S. Mansson, J. S. Petersson, C. M. Chai, G. Hansson, O. Axelsson, and K. Golman, "Passive catheter tracking during interventional MRI using hyperpolarized 13C," *Magn Reson Med,* vol. 57, pp. 1140-7, Jun 2007.

[9] V. D. Kochli, G. C. McKinnon, E. Hofmann, and G. K. Vonschulthess, "Vascular Interventions Guided by Ultrafast Mr-Imaging - Evaluation of Different Materials," *Magnetic Resonance in Medicine,* vol. 31, pp. 309-314, Mar 1994.

[10] E. Atalar, P. A. Bottomley, O. Ocali, L. C. L. Correia, M. D. Kelemen, J. A. C. Lima, and E. A. Zerhouni, "High resolution intravascular MRI and MRS by using a catheter receiver coil," *Magnetic Resonance in Medicine,* vol. 36, pp. 596-605, Oct 1996.

[11] O. Ocali and E. Atalar, "Intravascular magnetic resonance imaging using a loopless catheter antenna," *Magnetic Resonance in Medicine,* vol. 37, pp. 112-118, Jan 1997.

[12] E. Atalar, P. A. Bottomley, O. Ocali, L. C. Correia, M. D. Kelemen, J. A. Lima, and E. A. Zerhouni, "High resolution intravascular MRI and MRS by using a catheter receiver coil," *Magn Reson Med,* vol. 36, pp. 596-605, Oct 1996.

[13] M. Bock, S. Muller, S. Zuehlsdorff, P. Speier, C. Fink, P. Hallscheidt, R. Umathum, and W. Semmler, "Active catheter tracking using parallel MRI and real-time image reconstruction," *Magn Reson Med,* vol. 55, pp. 1454-9, Jun 2006.

[14] A. Buecker, G. B. Adam, J. M. Neuerburg, S. Kinzel, A. Glowinski, T. Schaeffter, V. Rasche, J. J. van Vaals, and R. W. Guenther, "Simultaneous real-time visualization of the catheter tip and vascular anatomy for MR-guided PTA of iliac arteries in an animal model," *J Magn Reson Imaging,* vol. 16, pp. 201-8, Aug 2002.

[15] C. L. Dumoulin, S. P. Souza, and R. D. Darrow, "Real-time position monitoring of invasive devices using magnetic resonance," *Magn Reson Med,* vol. 29, pp. 411-5, Mar 1993.

[16] L. Feng, C. L. Dumoulin, S. Dashnaw, R. D. Darrow, R. Guhde, R. L. Delapaz, P. L. Bishop, and J. Pile-Spellman, "Transfemoral catheterization of carotid arteries with real-time MR imaging guidance in pigs," *Radiology,* vol. 234, pp. 551-7, Feb 2005.

[17] C. M. Hillenbrand, D. R. Elgort, E. Y. Wong, A. Reykowski, F. K. Wacker, J. S. Lewin, and J. L. Duerk, "Active device tracking and high-resolution intravascular MRI using a novel catheter-based, opposed-solenoid phased array coil," *Magn Reson Med,* vol. 51, pp. 668-75, Apr 2004.

[18] O. Ocali and E. Atalar, "Intravascular magnetic resonance imaging using a loopless catheter antenna," *Magn Reson Med,* vol. 37, pp. 112-8, Jan 1997.

[19] C. O. Schirra, S. Weiss, S. Krueger, S. F. Pedersen, R. Razavi, T. Schaeffter, and S. Kozerke, "Toward true 3D visualization of active catheters using compressed sensing," *Magn Reson Med,* vol. 62, pp. 341-7, Aug 2009.

[20] S. Zuehlsdorff, R. Umathum, S. Volz, P. Hallscheidt, C. Fink, W. Semmler, and M. Bock, "MR coil design for simultaneous tip tracking and curvature delineation of a catheter," *Magn Reson Med,* vol. 52, pp. 214-8, Jul 2004.

[21] H. H. Quick, M. O. Zenge, H. Kuehl, G. Kaiser, S. Aker, S. Massing, S. Bosk, and M. E. Ladd, "Interventional magnetic resonance angiography with no strings attached: Wireless active catheter visualization," *Magnetic Resonance in Medicine,* vol. 53, pp. 446-455, Feb 2005.

[22] W. Froncisz, A. Jesmanowicz, and J. S. Hyde, "INDUCTIVE (FLUX LINKAGE) COUPLING TO LOCAL COILS IN MAGNETIC-RESONANCE-IMAGING AND SPECTROSCOPY," *Journal of Magnetic Resonance,* vol. 66, pp. 135-143, Jan 1986.

[23] M. Bilgen, B. Al-Hafez, Y. Y. He, and W. M. Brooks, "Magnetic resonance angiography of rat spinal cord at 9.4 T: a feasibility study," *Magn Reson Med,* vol. 53, pp. 1459-61, Jun 2005.

[24] H. H. Quick, H. Kuehl, G. Kaiser, S. Bosk, J. F. Debatin, and M. E. Ladd, "Inductively coupled stent antennas in MRI," *Magn Reson Med,* vol. 48, pp. 781-90, Nov 2002.

[25] H. Celik, A. Uluturk, T. Tali, and E. Atalar, "A catheter tracking method using reverse polarization for MR-guided interventions," *Magn Reson Med,* vol. 58, pp. 1224-31, Dec 2007.

[26] K. J. Anderson, A. J. Dick, and G. A. Wright, "Catheter Tracking with Phase Information," in *ISMRM*, Kyoto, 2004, p. 2960.

[27] J. H. Hwang, Y. Zhou, C. Warren, A. A. Brayman, and L. A. Crum, "Targeted Venous Occlusion Using Pulsed High-Intensity Focused Ultrasound," *Biomedical Engineering, IEEE Transactions on,* vol. 57, pp. 37-40, 2010.

[28] C. Di Mario, G. Gorge, R. Peters, P. Kearney, F. Pinto, D. Hausmann, C. von Birgelen, A. Colombo, H. Mudra, J. Roelandt, and R. Erbel, "Clinical application and image interpretation in intracoronary ultrasound. Study Group on Intracoronary Imaging of the Working Group of Coronary Circulation and of the Subgroup on Intravascular Ultrasound of the Working Group of Echocardiography of the European Society of Cardiology," *Eur Heart J,* vol. 19, pp. 207-29, Feb 1998.

[29] M. P. Fronheiser, E. D. Light, and S. W. Smith, "Real-time 3D ultrasound with multiple transducer arrays," in *Ultrasonics Symposium, 2004 IEEE*, 2004, pp. 786-789 Vol.1.

[30] H. Celik, A. Ulutürk, Y. Eryaman, T. Talı, and E. Atalar, "A Novel Catheter Tracking Method Using Reversed Polarization," in *14th Annual Meeting of ISMRM* Seattle, USA, 2006.

[31] M. Burl, G. A. Coutts, and I. R. Young, "Tuned fiducial markers to identify body locations with minimal perturbation of tissue magnetization," *Magn Reson Med,* vol. 36, pp. 491-3, Sep 1996.
[32] H. Quick, M. Zenge, H. Kuehl, G. Kaiser, S. Aker, H. Eggebrecht, S. Massing, and M. Ladd, "Wireless Active Catheter Visualization: Passive Decoupling Methods and Their Impact on Catheter Visibility," in *ISMRM* Miami Beach, Florida, USA, 2005.
[33] P. Aksit, J. A. Derbyshire, J. M. Serfaty, and E. Atalar, "Multiple field of view MR fluoroscopy," *Magnetic Resonance in Medicine,* vol. 47, pp. 53-60, Jan 2002.
[34] M. A. Guttman, R. J. Lederman, J. M. Sorger, and E. R. McVeigh, "Real-time volume rendered MRI for interventional guidance," *Journal of Cardiovascular Magnetic Resonance,* vol. 4, pp. 431-U1, 2002.
[35] E. Hayes CE, Schenck JF, Mueller OM, Eash M, "An efficient, highly homogenous radiofrequency coil for whole-body NMR imaging at 1.5 T," *J Magn Reson,* vol. 63., pp. 622–628, 1985.
[36] Signa; Excite, GE medical systems; Milwaukee, Wisconsin, USA.
[37] "ATC, Huntington Station, New York, USA."
[38] Agilent Technologies, Santa Clara, CA, USA.
[39] Infineon Tech.; Germany.
[40] C. J. Yeung, R. C. Susil, and E. Atalar, "RF safety of wires in interventional MRI: using a safety index," *Magn Reson Med,* vol. 47, pp. 187-93, Jan 2002.
[41] Neoptix, Inc., Quebec City, Canada.
[42] Decagon Devices, Inc. WA, USA.
[43] K. A. Shunk, J. A. Lima, A. W. Heldman, and E. Atalar, "Transesophageal magnetic resonance imaging," *Magn Reson Med,* vol. 41, pp. 722-6, Apr 1999.
[44] K. B. Baker, J. A. Tkach, J. A. Nyenhuis, M. Phillips, F. G. Shellock, J. Gonzalez-Martinez, and A. R. Rezai, "Evaluation of specific absorption rate as a dosimeter of MRI-related implant heating," *J Magn Reson Imaging,* vol. 20, pp. 315-20, Aug 2004.
[45] R. C. Susil, A. Krieger, J. A. Derbyshire, A. Tanacs, L. L. Whitcomb, G. Fichtinger, and E. Atalar, "System for MR image-guided prostate interventions: canine study," *Radiology,* vol. 228, pp. 886-94, Sep 2003.
[46] P. B. Roemer, W. A. Edelstein, C. E. Hayes, S. P. Souza, and O. M. Mueller, "The NMR phased array," *Magn Reson Med,* vol. 16, pp. 192-225, Nov 1990.
[47] G. H. Glover, C. E. Hayes, N. J. Pelc, W. A. Edelstein, O. M. Mueller, H. R. Hart, C. J. Hardy, M. O'Donnell, and W. D. Barber, "Comparison of linear and circular polarization for magnetic resonance imaging," *Journal of Magnetic Resonance (1969),* vol. 64, pp. 255-270, 1985.
[48] N. M. Knufman, P. A. van den Elsen, J. P. Cillessen, J. W. van Isselt, and C. A. Tulleken, "Spatial integration of multimodal brain images in cerebral infarction," *Brain Topogr,* vol. 5, pp. 165-9, Winter 1992.
[49] J. A. Maintz, P. A. Van den Elsen, and M. A. Viergever, " Registration of 3D medical images using simple morphological tools " in *Lecture Notes in Computer Science*. vol. 1230/1997: Springer Berlin / Heidelberg, 1997.
[50] J. B. Maintz and M. A. Viergever, "A survey of medical image registration," *Med Image Anal,* vol. 2, pp. 1-36, Mar 1998.
[51] P. A. Van den Elsen, J. A. Maintz, E. D. Pol, and M. A. Viergever, "Automatic registration of CT and MR brain images using correlation of geometrical features," *IEEE Trans Med Imaging,* vol. 14, pp. 384-96, 1995.
[52] M. A. Viergever, J. B. Maintz, W. J. Niessen, H. J. Noordmans, J. P. Pluim, R. Stokking, and K. L. Vincken, "Registration, segmentation, and visualization of

multimodal brain images," *Comput Med Imaging Graph,* vol. 25, pp. 147-51, Mar-Apr 2001.

[53] C. E. Hayes, W. A. Edelstein, J. F. Schenck, O. M. Mueller, and M. Eash, "An efficient, highly homogenous radiofrequency coil for whole-body NMR imaging at 1.5 T," *J Magn Reson,* vol. 63., pp. 622–628, 1985.

[54] D. I. Hoult, "The principle of reciprocity in signal strength calculations - A mathematical guide," *Concepts in Magnetic Resonance,* vol. 12, pp. 173-187, 2000.

[55] H. Vesselle and R. E. Collin, "The signal-to-noise ratio of nuclear magnetic resonance surface coils and application to a lossy dielectric cylinder model. I. Theory," *Biomedical Engineering, IEEE Transactions on,* vol. 42, pp. 497-506, 1995.

[56] S. M. Wright and L. L. Wald, "Theory and application of array coils in MR spectroscopy," *NMR Biomed,* vol. 10, pp. 394-410, Dec 1997.

[57] A. Reykowski and M. Blasche, "Mode matrix—a generalized signal combiner for parallel imaging arrays. In Proc. 12th Annual Meeting of the International Society for Magnetic Resonance in Medicine,," Kyoto, 2004, p. 1587.

[58] Z. Chen, L. A. Johnston, D. H. Kwon, S. H. Oh, Z. H. Cho, and G. F. Egan, "An optimised framework for reconstructing and processing MR phase images," *Neuroimage,* vol. 49, pp. 1289-300, Jan 15 2010.

[59] T. Cukur, M. Lustig, and D. G. Nishimura, "Multiple-profile homogeneous image combination: application to phase-cycled SSFP and multicoil imaging," *Magn Reson Med,* vol. 60, pp. 732-8, Sep 2008.

[60] K. P. Pruessmann, M. Weiger, M. B. Scheidegger, and P. Boesiger, "SENSE: sensitivity encoding for fast MRI," *Magn Reson Med,* vol. 42, pp. 952-62, Nov 1999.

[61] T. Cukur, J. M. Santos, J. M. Pauly, and D. G. Nishimura, "Variable-density parallel imaging with partially localized coil sensitivities," *IEEE Trans Med Imaging,* vol. 29, pp. 1173-81, May 2010.

[62] T. S. Ibrahim, R. Lee, A. M. Abduljalil, B. A. Baertlein, and P.-M. L. Robitaille, "Dielectric resonances and B1 field inhomogeneity in UHFMRI: computational analysis and experimental findings," *Magnetic Resonance Imaging,* vol. 19, pp. 219-226, 2001.

[63] U. Katscher, P. Börnert, C. Leussler, and J. S. van den Brink, "Transmit SENSE," *Magnetic Resonance in Medicine,* vol. 49, pp. 144-150, 2003.

[64] G. Adriany, P. F. Van de Moortele, F. Wiesinger, S. Moeller, J. P. Strupp, P. Andersen, C. Snyder, X. Zhang, W. Chen, K. P. Pruessmann, P. Boesiger, T. Vaughan, and K. Uğurbil, "Transmit and receive transmission line arrays for 7 Tesla parallel imaging," *Magnetic Resonance in Medicine,* vol. 53, pp. 434-445, 2005.

[65] R. G. Pinkerton, J. P. Near, E. A. Barberi, R. S. Menon, and R. Bartha, "Transceive surface coil array for MRI of the human prostate at 4T," *Magnetic Resonance in Medicine,* vol. 57, pp. 455-458, 2007.

[66] H. Celik, I. Mahcicek, and E. Atalar, "Catheter Tracking Using Transmit Array System," in *ISMRM*, Stockholm, 2010.

[67] H. Celik, I. Mahcicek, and E. Atalar, "TrueFISP Based Catheter Tracking Using a Transmit Array System," in *iMRI*, Leipzig, 2010.

[68] E. M. Haacke, R. W. Brown, M. R. Thompson, and R. Vanktatesan, *MRI Physical Principles and Sequence Design*. New York: Wiley-LISS, 1999.

[69] M. A. Bernstein, M. Grgic, T. J. Brosnan, and N. J. Pelc, "Reconstructions of phase contrast, phased array multicoil data," *Magn Reson Med,* vol. 32, pp. 330-4, Sep 1994.

[70] V. Acikel and E. Atalar, " Modeling of RF Induced Implant Lead Current for MRI," in *17th Annual Meeting of ISMRM* Honolulu, Hawaii, USA, 2009.

[71] H. Quick, M. Zenge, H. Kuehl, G. Kaiser, S. Aker, H. Eggebrecht, S. Massing, and M. Ladd, "Wireless Active Catheter Visualization: Passive Decoupling Methods and Their Impact on Catheter Visibility," in *13th Annual Meeting of ISMRM* Miami Beach, Florida, USA, 2005.

[72] H. Celik, H. Quick, M. Zenge, and E. Atalar, "Wireless Active Catheter Tracking Method Using Reversed Polarization: Implementation of 12-Channels Phased Array Coil," in *ESMRMB* Warsaw, Poland, 2006.